ACS Catalysis

pubs.acs.org/acscatalysis

Research Article

Supported Ni–Au Colloid Precursors for Active, Selective, and Stable Alkyne Partial Hydrogenation Catalysts

James E. Bruno, Nicolas S. Dwarica, Todd N. Whittaker, Emily R. Hand, Clemente S. Guzman, IV, Anish Dasgupta, Zhifeng Chen, Robert M. Rioux, and Bert D. Chandler*

Cite This: *ACS Catal.* 2020, 10, 2565–2580

Read Online

ACCESS | Metrics & More | Article Recommendations | Supporting Information

ABSTRACT: Bimetallic NiAu catalysts have garnered broad interest for a variety of reactions including automotive emissions, selective hydrogenation, selective oxidation, hydrodechlorination, and biomass conversion. However, the bulk immiscibility of the two metals, complicating catalyst synthesis, has limited studies of this bimetallic system. We report a solution-phase synthesis for Ni and bimetallic NiAu heterogeneous catalysts. Using oleylamine as a capping agent, an optimized synthesis for Ni catalysts led to supported particles with a narrow size distribution (4.7 ± 0.4 nm). Gold was added to the Ni nanoparticles via galvanic displacement of Ni in organic solution, the particles were deposited onto commercial alumina, and oleylamine capping agent was removed. The catalytic activity of the bimetallic materials in 1-octyne partial hydrogenation was in between the activity of monometallic Ni and Au catalysts. At high space velocity, the bimetallic catalysts largely maintained the high alkene selectivity associated with Au catalysts (>90% alkene selectivity at a 95% conversion). At lower space velocities, the NiAu catalysts also had a reduced propensity to overhydrogenate the alkene (relative to Ni). A simple catalyst performance parameter, which combined activity, selectivity, and space velocity, was developed and used to describe the overall performance of each catalyst under varying reaction conditions. By this metric, the bimetallic catalysts had considerably better performance than monometallic Ni. The most active bimetallic catalyst was examined with a week-long stability test; it showed no activity loss with a 100% carbon balance. Catalysts were characterized by transmission electron microscopy, X-ray diffraction, H_2 and N_2 adsorption, and inductively coupled plasma-optical emission spectroscopy (ICP-OES). The reactivity and characterization studies suggest the active catalysts are likely composed of bimetallic NiAu surfaces. The incorporation of Au into the catalysts suppresses H_2 adsorption on Ni, leading to lower hydrogen coverage during catalysis; this contributes to slowing undesirable alkene hydrogenation and improving catalyst selectivity.

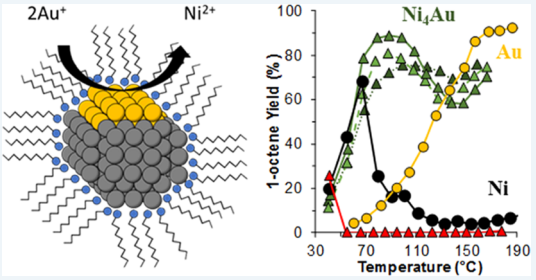

KEYWORDS: *alkyne semihydrogenation, colloid synthesis, Ni–Au, bimetallic catalyst, catalyst deactivation, reaction kinetics, catalyst performance, hydrogen adsorption*

INTRODUCTION

Industrial polyolefin feedstocks contain <5% alkynes or dienes (e.g., acetylene, propyne, or 1,3-butadiene).[1−6] The concentration of these impurities must be reduced to <10 ppm to prevent poisoning of downstream polymerization catalysts in plastic production. These impurities are generally removed through partial or selective hydrogenation of the polyunsaturated impurity into the corresponding alkene (for example, acetylene partial hydrogenation to ethylene for polyethylene production). The catalyst for this process has three key requirements: (1) high rates of acetylene hydrogenation to ethylene; (2) dramatically lower rates of ethylene hydrogenation to ethane; and (3) resistance to deactivation, which is typically due to the oligomerization of reactive unsaturated surface species. The second requirement is vitally important to protect the predominately olefin feed from hydrogenation and provide high alkene selectivity.[7,8]

Palladium and nickel are active hydrogenation catalysts[9] that have long been used by industry for alkyne partial (or semi) hydrogenation.[5,6,10] However, both metals have low intrinsic alkene selectivity, as they overhydrogenate ethylene to ethane at low temperatures (<50 °C). In addition, Ni is a particularly active oligomerization catalyst and generates oligomeric side products ("green oil") that deactivate the catalyst.[11−13] Various groups improved alkene selectivity using low Pd loading or Pd single sites.[14,15] Pd is also incorporated into PdM bimetallic catalysts to control catalyst selectivity and improve stability. Recent studies using PdZn alloys showed weaker alkene binding contributed to improved selectivity.[16,17] Both alkene selectivity and catalyst stability were further improved by preparing highly dilute Pd sites in Ga,[18] Cu,[19−24] Au,[25−32] and

Received: December 13, 2019
Revised: January 14, 2020
Published: January 15, 2020

https://dx.doi.org/10.1021/acscatal.9b05402
ACS Catal. 2020, 10, 2565–2580

Ag.[3,33] Of these, $PdAg/Al_2O_3$ is widely used for industrial partial alkyne hydrogenation.[10,34]

The rising cost of Pd has led to a renewed search for less expensive alkyne hydrogenation catalysts. Studt et al. identified Ni as a cheap, Earth-abundant alternative and suggested intermetallic NiZn materials as possible replacements for PdAg.[9] However, this study did not consider the impact of alkyne oligomerization. Spanjers et al. later synthesized well-controlled intermetallic NiZn catalysts and concluded ∼40% of acetylene was converted into oligomers; catalyst deactivation was tied to the production of these oligomers.[35] Other recent studies on Ni hydrogenation catalysts are focused on the generation of single site or bimetallic catalysts to improve selectivity and decrease oligomerization rates to improve stability.[36−38]

Gold has also attracted recent attention as an alternative to Pd, and acetylene hydrogenation studies over supported Au catalysts report characteristically high alkene selectivity, typically >80%.[39−42] Density functional theory (DFT) calculations by Segura and Pérez-Ramírez explained high selectivity on Au is due to substantial differences in the binding energy of ethylene and acetylene.[43] On a Au_{19} cluster, their results indicated ethylene binds very weakly (−0.01 eV) to Au, while acetylene readily adsorbs (−0.67 eV).[43] A DFT study by Hardacre, Hu, and co-workers similarly showed considerably weaker acetylene and ethylene adsorptions on Au and Au−Ni surfaces relative to those on Ni.[44] This weak ethylene binding allows the alkene to desorb from the surface before overhydrogenation occurs. Similar high intrinsic alkene selectivity over Au has also been reported for other partial hydrogenations, including 1-propyne,[1] 1,3-butadiene,[2,45,46] phenylacetylene,[4,47] and 1-octyne.[48]

While Au catalysts have high intrinsic selectivity, they suffer from significantly slower hydrogenation rates relative to Pd or Ni.[48] This low Au activity requires either high metal loadings (undesirable due to the cost of Au) or high reaction temperatures (often ≥200 °C) for high alkyne conversion.[39,40,42,49] Low alkyne hydrogenation rates over Au are attributed to slow hydrogen activation kinetics over low-coordinated Au sites and low hydrogen coverage on an alkyne-saturated Au surface.[41,48,50−52] Additionally, Au catalysts show poor stability over time,[39,40,46] although Masoud et al. found stability depends greatly on the chemistry of the metal oxide support.[46]

Bimetallic Au-based catalysts, which incorporate more active heterometals into Au nanoparticles (NPs), have shown promise for combining the high activity and selectivity components of both metals. Louis and co-workers showed that dilute Pd−Au alloys have improved 1,3-butadiene activity relative to Au and maintained favorable 1-butene selectivity.[30] Highly dilute Pd sites in Au were postulated to help improve H_2 activation kinetics, which are slow on Au surfaces.[53] Palladium and gold are completely miscible in the bulk, and bimetallic NPs are readily prepared through deposition−precipitation.[53,54] However, both Pd and Au are expensive precious metals, giving less expensive PdAg catalysts a considerable economic advantage.

On a per gram basis, Pd and Au are more than 1000× more expensive than Ni, which is a relatively active hydrogenation catalyst. This makes the NiAu system an attractive target for low-cost partial hydrogenation catalysts, particularly if it is possible to combine the activity of Ni with the selectivity of Au.[9,44,55]

Accordingly, there have been several recent studies exploring NiAu alloys for several industrially important reactions including (i) NO reduction with CO for automotive emission abatement,[56−59] (ii) selective hydrogenations, particularly of substituted nitroaromatics,[60−64] (iii) alkyne[65−67] and butadiene[68] partial hydrogenation, (iv) hydrodechlorination,[69] (v) allylbenzyne isomerization,[70] (vi) CO oxidation,[71−75] (vii) selective alcohol oxidation,[76] and (vi) the reduction of levulinic acid with formic acid to yield γ-valerolactone.[77] The Ni−Au system is particularly interesting for partial hydrogenation reactions. Gold has been suggested to improve selectivity over Ni-based catalysts,[44,65−67] and adding group VIII metals has been shown to improve hydrogenation activity over Au.[53,54,78] For alkyne partial hydrogenation and similar reactions, there is a strong likelihood for a synergy to arise when the two metals interact.

In spite of this potential and interest in a broad range of reactions, progress has been limited by catalyst preparation. Nickel and gold are completely immiscible in the bulk, and bimetallic nanoparticles have proven difficult to prepare via traditional impregnation routes. Louis et al. used deposition−precipitation to prepare bimetallic catalysts, and, while evidence of bimetallic particles was found, widespread phase segregation was observed.[68] Keane and co-workers initially resorted to reduction at a very high temperature (1000 °C) to access regions in the phase diagram where the components are miscible;[60,61,69] unsurprisingly, nanoparticle sintering was observed. They have since turned to reductive deposition of Au onto supported NiO/Ni materials,[61,62] as have others.[63,76,77] A two-step procedure to sequentially deposit and reduce Au and Ni onto aminosiloxane-modified silica has also been utilized to prepare bimetallic catalysts.[65,79]

Several groups have reported various colloidal syntheses, typically using polymeric capping agents.[56,59,64,71,80] However, capping agent removal led to significant sintering, and we are aware of only one report where particles are indicated to be smaller than 10 nm.[56] Bimetallic NiAu catalysts have also been prepared using pyrophoric butyllithium as a reducing agent and trioctylphosphine as colloid stabilizer;[81] however, soft ligands such as phosphines and thiols are notoriously difficult to remove from Au catalysts.[71,82,83] The Flytzani−Stephanopoulos group has also recently reported the production of Ni-decorated Au NPs from a colloidal Au precursor.[78] Gold-decorated Raney−Ni catalysts have also been reported.[84]

We recently adapted a colloidal synthesis method for Au NPs to prepare consistently sized 2−4 nm Au NPs on a variety of supports.[48] The development of oleylamine-based syntheses is particularly valuable for catalyst precursors, as oleylamine can be removed under relatively mild conditions (e.g., H_2 at ∼300 °C).[48] In this work, we extend our synthetic methodologies to the preparation of supported bimetallic NiAu catalysts. As we detail below, this methodology leads to catalysts with improved catalyst activity (relative to Au), improved selectivity (relative to Ni), and dramatically improved stability.

METHODS AND MATERIALS

Materials. Borane *tert*-butylamine (BTB, 97%), oleylamine (98%), oleic acid (90%), diphenyl ether (DPE, 99%), HCl (37%, reagent grade), HNO_3 (70%, reagent grade), and SiC (≥97.5%, 400 mesh) were purchased from Sigma-Aldrich and used as received. Ni(acetylacetonate)$_2$ (Ni(acac)$_2$) was prepared according to literature procedures.[85] $HAuCl_4 \cdot 3H_2O$

https://dx.doi.org/10.1021/acscatal.9b05402
ACS Catal. 2020, 10, 2565−2580

was prepared by dissolving a certified Canadian Gold Leaf gold coin (99.99% Au) in freshly prepared aqua regia. Concentrated HCl was then added and removed by slow evaporation (3×); cooling yielded orange crystals of $HAuCl_4 \cdot 3H_2O$.[86] The Al_2O_3 support, Puralox HP 14/150 (Sasol), was calcined at 500 °C for 16 h prior to catalyst preparation. The NiO support was synthesized from $Ni(NO_3)_2$ through a modified Pechini process described in our previous work.[48] Commercially available catalysts included a Ni/Al_2O_3 catalyst (NIH Ni/Al_2O_3, 20 wt % NiO, UNICAT) and 0.8 wt % Au/Al_2O_3 (STREM) catalyst.

Catalyst Precursor Synthesis. All syntheses were performed using standard air-free Schlenk techniques. To prepare the Ni nanoparticles (NPs), a scrupulously dried 250 mL three-necked round-bottom flask was charged with 514 mg $Ni(acac)_2$, 3.8 mL oleic acid, 22 mL DPE, and 8 mL oleylamine, followed by evacuation and purging with N_2. The $Ni(acac)_2$ solution was further purged at 120 °C under flowing N_2 for 90 min while stirring at 800 rpm. The solution was confirmed to be free of water when the color of the solution changed from light blue to green. The solution was then rapidly heated to 170 °C.

In a separate Schlenk flask, 522 mg BTB was dissolved in 1.5 mL DPE and 0.5 mL oleylamine with mild heating. The BTB solution was withdrawn into a scrupulously dried glass syringe with an 18 gauge needle and injected by hand into the $Ni(acac)_2$ solution at 170 °C to initiate Ni reduction and particle nucleation. The entire volume (2 mL) was added within 1 s and an instantaneous color change from light green to black confirmed the reduction of Ni(II) to Ni(0). The colloidal solution was held at 170 °C for 10 min, removed from the heat, and quenched with a dry, room-temperature solution of 2.5 mL oleylamine in 7.5 mL DPE. The addition of the dry solvent (via glass syringe with a 22 gauge needle) over ∼5 s rapidly cooled the reaction solution to 50 °C. To prepare the monometallic Ni catalyst, the Ni NP colloids were deposited onto an alumina support by stirring overnight under N_2 at 25 °C.

The bimetallic catalyst precursors were prepared via galvanic exchange immediately after the cooling step in the Ni colloid synthesis.[87] A Au(I) solution was prepared by purging 570 mg $HAuCl_4 \cdot 3H_2O$ with N_2 followed by the addition of 10 mL oleylamine and 20 mL DPE. The solution was heated in a water bath to 65 °C under N_2 purge; the reduction of Au(III) to Au(I) was indicated by the color change from dark orange to light yellow. Varying volumes of this Au solution were added to the Ni colloids via cannula transfer over the course of 10 min; the solution was then stirred at 50 °C for an additional 50 min. The resulting NPs were cannula-transferred to a Schlenk flask containing freshly calcined Al_2O_3. The slurry was stirred overnight under N_2 at 25 °C to ensure complete deposition of the NPs. The $NiAu/Al_2O_3$ materials were then filtered, washed with acetonitrile, and stored at 4 °C in air. Monometallic Au catalysts supported on Al_2O_3 and NiO were also prepared using our adaptation of Sun and co-worker synthesis of oleylamine-capped Au NPs,[87] as previously described.[48]

Catalyst Characterization. Colloidal ("c-") catalysts included c-Au/Al_2O_3, c-Ni/Al_2O_3, and three c-Ni_xAu/Al_2O_3 (x = 2−4). The capping ligands were removed prior to characterization by heating to 300 °C for 1 h under flowing H_2/N_2 (100 mL/min, 50% v/v), as previously reported for monometallic Au catalysts.[48] Two industrial catalysts were also tested: NIH Ni/Al_2O_3 (UNICAT) and STREM Au/Al_2O_3. The NIH Ni/Al_2O_3 catalyst was reduced at 150 °C for 16 h under the same flow conditions prior to testing.

Elemental composition was determined with inductively coupled plasma-optical emission spectroscopy (ICP-OES, Varian 720-ES). Approximately 50 mg of catalyst was digested at 80 °C in 10 mL of aqua regia. The sample was magnetically stirred at 400 rpm for 3 days. The dissolved metals were diluted 10:1 in deionized water before analysis.

N_2 physisorption and H_2 adsorption experiments were performed on a Micromeritics ASAP 2020 instrument. For N_2 physisorption, approximately 200 mg of catalyst was degassed at 200 °C for 1 h at 10 μm Hg. Data were collected at 77 K, and surface areas were calculated with the Brunauer−Emmett−Teller (BET) method. For H_2 adsorption measurements, approximately 400 mg of previously pretreated catalyst (i.e., capping agents had previously been removed) was pretreated in situ for 16 h at 150 °C under a flowing H_2. The sample was then evacuated at 150 °C for 30 min and cooled to 30 °C under an active vacuum. A series of two isotherm H_2 adsorption experiments were then performed. The pressure range for both total and reversible adsorption isotherms was 1−600 mm Hg H_2; the sample was evacuated to at least 10 μm Hg for 1 h at the adsorption temperature between isotherms. After collection of the second (reversible adsorption) isotherm, the sample was treated again for 1 h at 150 °C under a flowing H_2, evacuated at 150 °C for 30 min, and cooled to the next adsorption temperature. This process was repeated for adsorption temperatures of 30, 60, 90, and 120 °C. Heats of adsorption were determined using two linearized versions of the Langmuir adsorption equation.

Monometallic Ni/Al_2O_3 and bimetallic $NiAu/Al_2O_3$ catalysts were imaged with scanning/transmission electron microscopy (STEM) using an FEI Talos F200X microscope at an accelerating voltage of 200 kV. Energy-dispersive spectrometry (EDS) measurements were conducted on the Talos microscope using a superX EDS detector. A small quantity of each sample was crushed in an agate mortar and dispersed in ethanol with sonication. A few drops of this suspension were placed on a Cu TEM grid (Electron Microscopy Science Inc.) and allowed to dry before inserting into the microscope for analysis. The number-averaged diameter for monometallic Ni and bimetallic Ni−Au nanoparticles was determined with ImageJ from the measurement of >100 particles. Error bars associated with the diameter represent the standard deviation of the distribution.

Powder X-ray diffraction was performed on Ni−Au NPs on a PANalytical Empyrean II diffractometer using a Co Kα radiation. The incident optics consisted of a 1/8° divergence slit, a 10 mm beam mask, a 1/2° antiscatter slit, and a 0.04 rad soller slit. The detector optics consisted of an X'celerator detector with 0.04 rad soller slits. Data was collected in the 2θ range of 10−120°.

Light-Off Curves and Kinetics Studies. Catalysts were evaluated for 1-octyne partial hydrogenation in a single-pass packed bed reactor. The appropriate mass of catalyst (see below) was diluted with 1.0 g SiC and loaded into a borosilicate reactor. The reactor was fitted with a thermocouple, loaded into a furnace, and H_2 and N_2 flow rates were set to 50 mL/min each with mass flow controllers (MFCs). Product gases were analyzed with an in-line GC/FID (SRI 8610C, 1 m packed silica gel column).

Once the reaction temperature was stable for 15 min, alkyne was introduced by flowing 10 mL/min of H_2 through a two-

https://dx.doi.org/10.1021/acscatal.9b05402
ACS Catal. 2020, 10, 2565−2580

Scheme 1. Ni NP Colloidal Synthesis and Subsequent Support Deposition

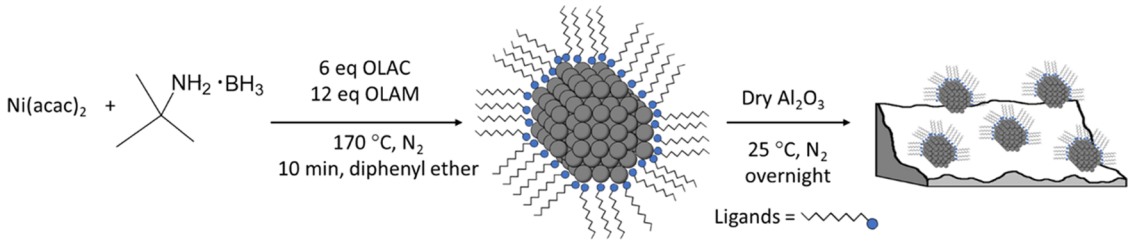

stage stainless steel saturator. The first stage contained 1-octyne at room temperature; the second stage was submerged in a condensing bath (−20 °C). The feed gas was then diluted with H_2 to 50 mL/min total with a second MFC, which yielded a 1-octyne feed pressure of 20 Pa (200 ppm). The gas hourly space velocity (GHSV) was ∼9700 h^{-1} in all tests based on the total mass of both the catalyst and the SiC diluent (∼1.0 g total). The GHSV calculated on the basis of catalyst mass ranged from 12 000 h^{-1} (100 mg catalyst) to 12 000 000 h^{-1} (0.1 mg catalyst); GHSVs for individual tests are reported in the figure caption. For light-off curves, Arrhenius plots, and 1-octyne order plots, the second H_2 MFC was set to 40 mL/min to achieve a total flow of 40 mL/min; for H_2 order plots, a mixture of H_2/N_2 was used to dilute the feed coming from the saturators.

Light-off curves were measured with 5−6 mg of the supported catalyst, ramping the furnace from 40 to ∼180 °C at a rate of 0.7 °C/min; product gases were analyzed every 15 min via GC/FID. Additional light-off curves were measured with 1−5 mg catalyst so that all catalysts could be compared on a consistent Au or Ni basis. For the commercial Ni catalyst, 1 mg of the catalyst was diluted in 10 g of SiC and mixed with a vortex mixer; light-off curves were determined with 1.0 g of the diluted mixture (∼0.1 mg NIH catalyst in the reactor).

Kinetic parameters were determined with fresh diluted catalysts under differential conversion. The mass for both NIH Ni and c-Ni was approximately 0.1 mg (GHSV = 12 000 000 h^{-1}); the mass for all other catalysts was 2−10 mg (GHSV ranged from 120 000 to 1 200 000 h^{-1}). Arrhenius plots and 1-octyne order plots were measured sequentially using the same sample of catalyst; the H_2 order determination occurred in a separate experiment. For the Arrhenius plot, 50 mL/min H_2 and 20 Pa 1-octyne flowed over the catalyst at 45, 50, 55, and 60 °C. The 1-octyne order plot was measured at 60 °C with four different condenser temperatures between −20 and 10 °C (∼20−200 Pa 1-octyne). The H_2 order was determined at 60 °C with a fresh sample of the catalyst under 50 mL/min H_2/N_2 and 20 Pa 1-octyne. The H_2 quantity in the feed gas was varied between 40 and 100 vol % H_2 (balance N_2). In-line gas samples were automatically injected into the GC every 15 min. Each data point reported is the average of four samples collected over 1 h.

There was a small amount of activity loss (typically <15%) due to catalyst deactivation over the course of the kinetics determination(s). This was accounted for in two ways. First, individual data points in the reaction order studies were determined in random order. Second, conditions for the first data point were retested at the end of the experiment, and the measured rates for the intervening data points were normalized assuming a linear loss of activity.

Stability tests were evaluated with a 0.7−2.5 mg catalyst, which was diluted, pretreated, and cooled to 110 °C. The catalyst mass for c-Ni_xAu was chosen so that the initial conversion was 15−20% at a pressure of ∼20 Pa 1-octyne (balance of the 50 mL/min flow rate was H_2); the mass of Ni and Au monometallic catalysts matched the molar loading of metals in c-Ni_xAu. The GHSV ranged from 570 000 to 1 700 000 h^{-1} on the basis of these catalyst masses. Time-on-stream behavior was tracked for either 20 or 168 h (1 week); automated GC sampling took place every 15 min.

RESULTS AND DISCUSSION

Synthesis of Oleylamine-Capped Ni and NiAu Catalyst Precursors. Nickel−gold systems are not well studied due to the bulk immiscibility of Ni and Au. Our synthetic goal was to develop a new route to supported bimetallic NiAu catalysts allowing for further study of this system. Since our target is a supported catalyst, our nanoparticle synthesis was developed with the understanding that the capping agents will ultimately be sacrificed during catalyst activation. We therefore developed our methodologies using oleylamine as a capping agent. Oleylamine (OLAM) is inexpensive, commercially available, and has a moderate boiling point (364 °C). This provides a significant advantage over stabilizers such as dendrimers, poly(vinyl alcohol), and poly(vinylpyrrolidone), which must be removed via an oxidative process to prepare active catalysts.[83,88−90] Avoiding the deposition of oxidized capping ligand decomposition products may be particularly advantageous for Au-based systems because the catalytic activity of supported Au NPs often depends on the chemistry both at and near the metal−support interface (MSI).[48,52,91] OLAM can be removed directly via evaporation/desorption, which should dramatically reduce the deposition of partially oxidized organic residues (e.g., carbonates).[82,89]

We first developed a Ni colloid synthesis, informed by recent studies from the Murray and Sun groups. Murray and co-workers developed a synthesis for preparing monodisperse 4−12 nm Ni colloids, where they achieved particle size control by varying the reaction temperature and capping ligand concentration.[92] However, their use of phosphine-based ligands is undesirable for heterogeneous catalyst synthesis due to the potential for depositing residual phosphorous species. Sun and co-workers developed a low-temperature procedure where borane *tert*-butylamine (BTB) was employed to reduce $Ni(acac)_2$ and form Ni NPs.[93] While small (4−12 nm), monodisperse Ni NPs can be prepared by this synthesis,[92] attempts to synthesize larger particles resulted in broad particle size distributions. These results motivated our synthetic approach in which we sought to use only OLAM and oleic acid (OLAC) capping ligands. Relatively mild reaction temperatures (<200 °C) were enabled using BTB as the reductant (Scheme 1).

https://dx.doi.org/10.1021/acscatal.9b05402
ACS Catal. 2020, 10, 2565−2580

Screening studies for Ni NP synthesis conditions and resulting particle sizes are summarized in Table 1. Freshly prepared colloidal Ni NPs were immediately deposited on alumina supports and washed with dry acetonitrile to remove solvent and excess ligands. TEM measurements were made after the removal of capping ligands to evaluate the particle size distribution. The materials were all exposed to air after capping agent removal; so, Ni oxidation is expected (and confirmed by XRD); for simplicity, we express all of the particle sizes below simply as Ni(NiO). Control over Ni(NiO) NP size from 3 to 7 nm was initially achieved by varying both the Ni(II) reduction time and temperature (Table 1, batches A–D). Shorter reaction times and higher reaction temperatures favored the formation of smaller NPs with moderate control over size dispersion. A significant narrowing of the Ni(NiO) NP size distribution was further achieved by increasing BTB and OLAC concentrations (batches E and F; additional STEM images available in the Supporting Information). These factors likely improved Ni solubility and accelerated the rate of Ni nucleation. Batch F gave excellent control over both particle size and distribution (4.7 ± 0.4 nm, Figure 1) and was therefore used in subsequent Ni and NiAu catalyst syntheses.

Our goal was to initially force interactions between Ni and Au in the bimetallic catalyst precursors. We therefore used galvanic displacement to exchange a fraction of the surface Ni with Au to generate bimetallic NiAu NPs in solution. This was accomplished by adding a Au(I)–oleylamine complex solution to freshly synthesized Ni NPs (Batch F, Table 1). Elemental analysis of the deposited NPs shows a smaller Ni/Au ratio than was used in the synthesis, which suggests a net loss of Ni during catalyst preparation (Table 2).

Structural Characterization. Powder XRD patterns of the c-NiAu catalysts, collected in air, are shown in Figure 2. The primary peaks were fitted to reference patterns for the Al_2O_3 support (2θ = 54.0, 79.7, 103.3°), oxidized Ni ($Ni_3O_2(OH)_4$), 23.0, 38.3, 43.8, 72.1°), and Au (45.8, 95.0°). There is also a weak, broad reflection at 61.1° that might be associated with a mixed NiAu phase. Keane and co-workers observed a single sharp reflection at $2\theta \approx 43°$ in their samples and assigned it to a NiAu alloy;[60] however, the reflection that we observe is far too weak to definitively assign.

The XRD data of the bimetallic catalysts show no Ni(0); small Ni NPs are well known to readily oxidize in air;[94] so, it is not surprising that Ni is present in an oxidized, hydrated phase. The reflections associated with Au are weak and broad (some are obscured by the $Ni_3O_2(OH)_4$ reflections), indicating that Au is well dispersed throughout the catalyst (i.e., there are few if any large monometallic Au NPs). Diffraction from small (~2 nm) Au NPs is typically not detectable in powder XRD; our previous work with 2–4 nm c-Au supported on Al_2O_3, SiO_2, and TiO_2 showed no Au diffractions, similar to the data in Figure 2.[48]

Table 1. Summary of Ni NP Synthesis Conditions and Resulting Particle Sizes

batch	eq. OLAC	eq. BTB	time (min)	temp (°C)	size[a] (nm)
A	1	1	5	160	5.8 ± 1.0
B	1	1	5	170	4.5 ± 0.8
C	1	1	5	180	3.2 ± 0.8
D	1	1	10	180	6.8 ± 1.5
E	3	2	6	170	3.4 ± 0.4
F	6	3	10	170	4.7 ± 0.4

[a]Particle sizes were determined by TEM after exposure to air and therefore represent oxidized Ni.

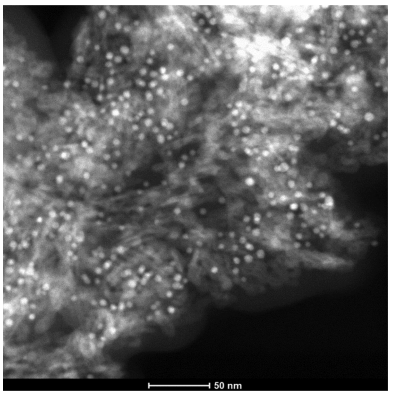

Figure 1. Representative STEM micrograph of c-Ni/Al_2O_3 catalyst, prepared with the procedure outlined in batch F of Table 1. The bright spots correspond to Ni; the gray background is the alumina support.

Representative TEM images for each bimetallic catalyst, along with STEM/energy-dispersive X-ray (EDS) elemental mapping studies, are provided in Figure 3; histograms for the particle size distributions are available in the Supporting Information. The c-NiAu catalysts have average particle diameters of about 8 nm with standard deviations between 3 and 4 nm (Table 2). These are larger particles and broader distributions than were observed for either the c-Ni or c-Au catalyst, indicating that the galvanic displacement step in the synthesis induced NP growth. However, these particles are significantly smaller than most previous reports for the NiAu system.[59,60,64,95]

Figure 3 also shows the representative EDS data; additional EDS mapping images are available in the Supporting Information. The Ni is primarily present in the larger particles; based on the XRD data, these are oxidized/hydrated forms of NiO. Small (1–4 nm) Au particles are distributed across the support, as suggested by the XRD data. There was also evidence of Ni dispersed across the support in some images. The elemental mapping data shows that the NiO phases are, in general, closely associated with Au; in many cases, the NiO particles appear to be decorated with small Au nanoparticles. This intermixing varies widely, with some NiO particles having very little associated Au and others nearly completely covered with Au. This wide range in the degree of Ni and Au associations, coupled with the variance in Au dispersion across individual images, resulted in no obvious distinguishing features for any of the individual bimetallic catalysts.

The structural characterization data must be considered in proper context, taking into account that they are collected after exposure to air. The close intermixing of the NiO and Au phases suggests we successfully prepared NiAu nanoparticles but the Ni rapidly oxidizes after deposition and exposure to air. Thus, the characterization data are best considered as representative of catalyst precursors; these data only indirectly describe the active catalysts, which undergo in-situ reduction.

While the c-NiAu particles are larger than the monometallic catalysts, the metals are well dispersed on the alumina surface and the c-NiAu particles are significantly smaller than most previous reports for the NiAu system.[59,60,64,95] More importantly, the colloidal synthesis forces close interactions

https://dx.doi.org/10.1021/acscatal.9b05402
ACS Catal. 2020, 10, 2565–2580

Table 2. Catalyst Characterization Data[a]

catalyst[a]	eq. Au in synthesis	Ni (wt %)	Au (wt %)	Au (mol %)	eq. Au in catalyst	size (nm)
c-Ni/Al_2O_3		1.4				4.7 ± 0.4
c-Ni_4Au/Al_2O_3	0.17	1.0	0.9	20	0.27	7.7 ± 4.6
c-Ni_3Au/Al_2O_3	0.24	2.1	2.3	25	0.33	7.4 ± 3.5
c-Ni_2Au/Al_2O_3	0.31	1.6	2.2	30	0.41	8.5 ± 3.8
c-Au/Al_2O_3			1.3	100		1.9 ± 0.3

[a]The BET surface areas were all between 130 and 140 m^2/g.

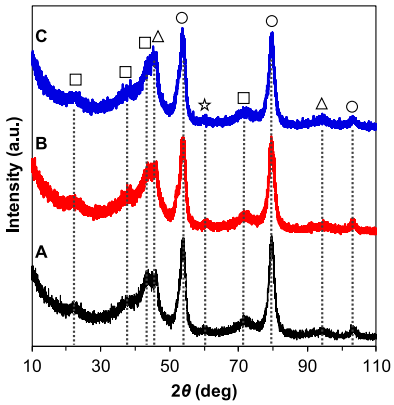

Figure 2. XRD for (A) c-Ni_4Au, (B) c-Ni_2Au, and (C) c-Ni_3Au. (○) $Al_{0.666}O$ (JCPDS file no. 98-001-2914), (□) $Ni_3O_2(OH)_4$ (JCPDS file no. 00-006-0144), (Δ) Au (JCPDS file no. 98-001-6186), and (☆) Au_3Ni (JCPDS file no. 04-016-1987).

between Ni and Au in the supported materials. While there is room for improvement with respect to preparing compositionally consistent particles, this degree of intermixing is significantly better than what is possible through traditional preparation methods.[59,60,64,95] Additionally, the synthesis utilizes only oleylamine capping agents, which are readily removed by treating under a flowing H_2 or N_2 at 300 °C. Infrared spectroscopy confirmed the removal of oleylamine from the c-Ni catalyst (see the Supporting Information); details on capping agent removal from Au catalysts were previously reported.[48] As we show below, this results in significantly improved catalytic performance relative to either monometallic catalyst.

Light-Off Curves and Selectivity at High Space Velocity. The primary industrial interest in alkyne partial hydrogenation is for selectively converting alkyne impurities to alkenes, i.e., as a purification catalyst. In a practical setting, the reaction is conducted at very high alkyne conversions (>99.9%), ideally with minimal secondary reaction of the alkene on the catalyst. Differential reaction kinetics, therefore, are not the most important measure of catalyst performance; rather, alkene selectivity at high conversion is a more valuable catalyst performance metric. Light-off curves, which measure conversion as a function of temperature under a specific set of reaction conditions, are particularly useful in this regard. We

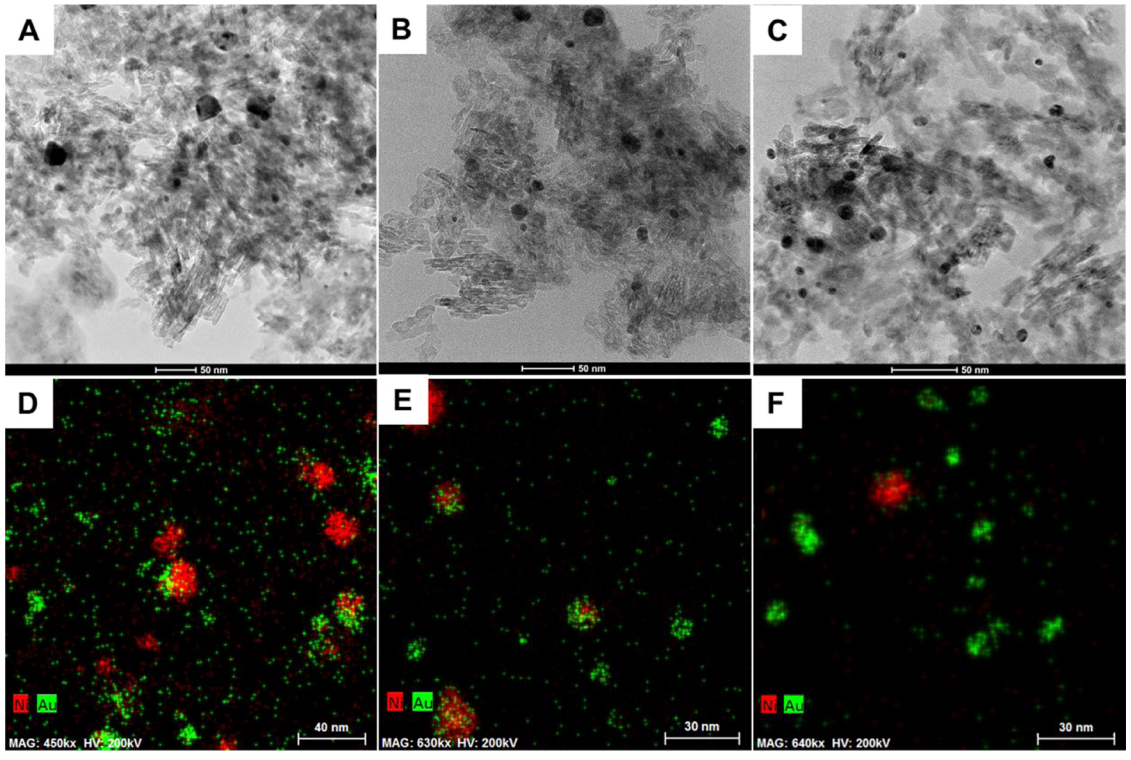

Figure 3. TEM images (A–C) and STEM/EDS images (D–F) of the bimetallic catalysts. (A) and (D) are c-Ni_4Au; (B) and (E) are c-Ni_2Au; and (C) and (F) are c-Ni_3Au.

https://dx.doi.org/10.1021/acscatal.9b05402
ACS Catal. 2020, 10, 2565–2580

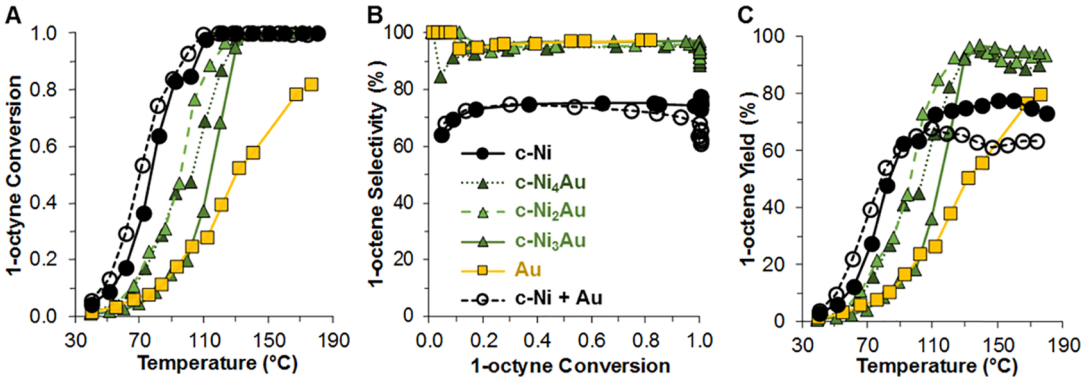

Figure 4. High space velocity catalysis data. (A) Light-off curves, (B) selectivity plots, and (C) yield plots for bimetallic c-NiAu/Al_2O_3 catalysts and alumina-supported monometallic catalysts. Conditions: 50 mL/min H_2, 20 Pa 1-octyne.

Table 3. Differential Conversion Kinetics Parameters for 1-Octyne Hydrogenation

	reaction orders[a]						
catalyst	1-octyne	H_2	$k_{obs\text{-}Au}$ [b,c]	$k_{obs\text{-}Ni}$ [b,d]	$k_{obs\text{-}H}$ [b,e]	E_{app} (kJ/mol)	intrinsic alkene selectivity (%)[f]
c-Ni/Al_2O_3	−0.1	1.1		170 ± 20	2700 ± 300	60 ± 4	75
c-Ni_4Au/Al_2O_3	−0.1	1.0	10 ± 0.1	2.7 ± 0.03	240 ± 10	40 ± 2	95
c-Ni_3Au/Al_2O_3	−0.1	1.1	9.1 ± 0.7	3.0 ± 0.3	650 ± 60	63 ± 3	95
c-Ni_2Au/Al_2O_3	−0.1	1.2	1.9 ± 0.1	0.78 ± 0.04	190 ± 10	56 ± 2	97
c-Au/Al_2O_3	−0.2	0.9	2 ± 1		50 ± 3	38 ± 1	98

[a]All reaction orders had standard errors of ±0.1 or smaller. [b]Conditions: 50 mL/min H_2, 20 Pa 1-octyne, 60 °C. [c]k_{obs} units: $\mu mol_{1\text{-octene}}\ [H_2]^{-1.0}\ mol_{Au}^{-1}\ min^{-1}$. [d]$k_{obs}$ units: $\mu mol_{1\text{-octene}}\ [H_2]^{-1.0}\ mol_{Ni}^{-1}\ min^{-1}$. [e]$k_{obs}$ units: $\mu mol_{1\text{-octene}}\ [H_2]^{-1.0}\ mol_{Hads}^{-1}\ min^{-1}$. [f]Does not account for nonvolatile oligomerization products.

primarily use light-off curves to evaluate selectivity as a function of conversion; however, they also provide a qualitative measure of activity over a wide temperature range. Consequently, we use the term "activity" here to compare temperatures required to achieve high (>85%) alkyne conversion; this is a qualitative comparison of performance, and no attempt is made to correct for metal loading(s) or dispersion. More precise alkyne hydrogenation activity measurements under differential conversion conditions are reported below.

The c-Ni and c-Au catalysts were first compared to commercial catalysts. Activity and selectivity plots for this comparison are available in the Supporting Information. In both cases, the commercial and colloidal catalysts showed similar reactivity and selectivity profiles. Thus, the colloidal synthesis, including capping agent removal, yields materials reasonably similar to traditionally prepared catalysts with no deleterious effects from the synthetic methodologies.

It is not possible to maintain constant Ni and Au loadings in the reactor for catalysts with different metal stoichiometries. Tests were therefore performed with masses of catalyst that allowed for relatively consistent amounts of Ni (0.3−0.5 μmol) and Au (0.10−0.15 μmol) in the reactor for each experiment. This corresponded to space velocities ranging from 45 to 70 mol C_8H_{14}/(mol metal h); for the bimetallic catalysts, the reported flow rates are normalized to the total amount of metal (Ni + Au) in the catalyst. These light-off curves are shown in Figure 4A. As expected, c-Ni appears more active than c-Au under these conditions, as the conversion reaches 100% at lower temperatures. For Ni, the activity is likely limited by overly strong alkyne binding, which reduces the number of sites available for H_2 activation;[44] for Au, the reaction is likely limited by weak H_2 adsorption.[48]

Alkene selectivity data collected during the light-off curve measurements are shown in Figure 4B. These selectivity profiles are fairly flat from ∼20 to 80% conversion; for convenience, we define the "intrinsic selectivity" of each catalyst as the average selectivity from 30 to 70% conversion. In this range of conversion, the catalyst surface is predominately covered in alkyne; so, this parameter largely describes the inherent reactivity of the alkyne under these conditions. The intrinsic alkene selectivity for c-Ni is 75%, while c-Au's intrinsic alkene selectivity is 98%. The high alkene selectivity of Au is associated with both weak alkene-Au binding[43] and low hydrogen coverage on Au catalysts.[41,51] These factors help to suppress the overhydrogenation of alkenes into alkanes over Au, resulting in high alkene selectivity.

The bimetallic catalysts exhibit consistently high intrinsic alkene selectivity (95−97%; Figure 4B and Table 3). This intrinsic selectivity is significantly higher than Ni and is generally comparable to the Au catalyst. Qualitatively, bimetallic catalyst activity was lower than c-Ni but higher than Au (Figure 4A). As conversion approached 100%, alkene selectivity over the bimetallic catalysts dropped to ∼85% due to overhydrogenation to octane. Similar selectivity loss occurs with the c-Ni catalyst, which drops below 60% alkene selectivity. The 1-octene yields of the c-NiAu catalysts are >80% over a large temperature range (∼80 °C); neither monometallic catalyst exhibited this performance under these conditions.

Figure 4 also includes data for a control experiment, consisting of a physical mixture of the c-Ni and STREM Au catalysts (0.4 μmol each metal) tested under the same flow conditions. The STREM Au catalyst was chosen because it is slightly more active than the c-Au catalyst. The light-off curve

https://dx.doi.org/10.1021/acscatal.9b05402
ACS Catal. 2020, 10, 2565−2580

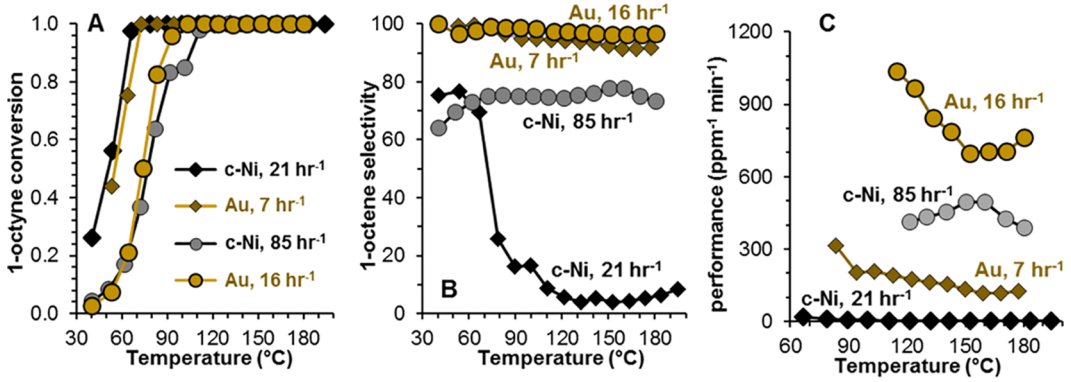

Figure 5. Monometallic catalyst light-off curve data showing the effect of space velocity and temperature on (A) 1-octene conversion, (B) 1-octene selectivity, and (C) catalyst performance (see the text for description). For clarity, performance data are only shown for 1-octyne slips <5 ppm. Reaction conditions: 50 mL/min H_2, 20 Pa 1-octyne; molar space velocities are noted in each panel. All catalysts were supported on Al_2O_3.

shows that the conversion, selectivity, and yield of the physical mixture were essentially the same as the more active c-Ni catalyst.

There are two important conclusions from this experiment. First, for this reaction, only the most active sites on the catalyst are the most important in determining catalyst activity and selectivity. In the particular case of the physical mixture, any catalysis by the Au particles was too slow to be detected relative to the Ni catalyst. Second, these results provide strong evidence that catalysis over the c-NiAu materials occurs on bimetallic NPs. If the c-NiAu catalysts underwent phase segregation during reduction, the bimetallic catalysts would exist as distinct Au NPs and Ni NPs on the surface, and the c-NiAu activity and selectivity would be similar to c-Ni. The high selectivity of the c-NiAu catalysts (relative to Ni) coupled with the higher activity (relative to Au) is therefore attributable to interactions between the two metal components driven by the colloidal synthesis.

Catalyst Performance at Low Space Velocities. Industrial partial hydrogenation catalysts operate in a large excess of alkene; consequently, reaction selectivity is largely governed by the alkene hydrogenation activity (often termed overhydrogenation). While a full examination of the industrial reaction under these conditions is beyond the scope of this fundamental study, evaluating a catalyst's propensity for overhydrogenation remains important. An evaluation of this catalyst property is readily obtained by collecting light-off curves at lower space velocities. The goal of these experiments is to increase the contact time between product alkenes and the catalyst surface. In simple terms, the reaction is run under conditions where most of the alkyne hydrogenation occurs in the first part of the catalyst bed, thus leaving the last portion of the bed exposed primarily to an alkene + H_2 atmosphere.

Catalyst operating conditions, such as feed composition and space velocity, can have large effects on catalyst performance. Because the space velocity is a normalized flow rate, it effectively describes the amount of time the feed spends over the catalyst (residence time is proportional to 1/SV; so, larger space velocity implies shorter reaction time). Most homogeneous catalysts convert more reactants to product given longer reaction times; comparatively, most heterogeneous catalysts foster higher conversion when operated at lower space velocities. Space velocity is particularly important for purification reactions such as alkyne partial hydrogenation, which are nominally sequential in nature (alkyne reacts first, then alkene). In this case, lower space velocities lead to longer contact between the catalyst and the initial octene product, which provides opportunities for undesired overhydrogenation of octene to octane.

Figure 5 presents light-off curve data showing the effects of space velocity on monometallic catalyst performance. As Figure 5A shows, space velocities for each metal can be chosen such that conversions are comparable at all temperatures. This has significant consequences for selectivity over the c-Ni catalyst, which essentially drops to 0 due to overhydrogenation (panel B). This effect also occurs for the Au catalyst but to a far lesser extent as selectivity remains above 90% at the lower space velocity. We note that oligomerization processes, which are pronounced for Ni catalysts,[96] are not included here due to their low volatility.

The activity and selectivity data can be combined into a single performance parameter or figure of merit (FOM). As we have previously shown,[97] such metrics can be useful in describing the key aspects of catalyst performance under widely varying reaction conditions. For 1-octyne partial hydrogenation, we define catalyst performance as follows

$$\text{performance FOM} = \frac{[P_{\text{alkyne}}][\text{SV}][S]}{[P_{\text{alkane}}][\text{alkyne slip (ppm)}]}$$

where P_{alkyne} is the 1-octyne pressure in the feed (20 Pa), SV is the molar space velocity, S is the alkene selectivity, P_{alkane} is the pressure of alkane leaving the reactor (i.e., the pressure of overhydrogenated alkyne), and alkyne slip is the amount of alkyne leaving the reactor.

This expression combines three essential elements of catalyst performance: reaction conditions, activity, and selectivity. Reaction conditions are broadly expressed by the alkyne pressure and space velocity; operating at high values of both parameters is desirable. Catalyst activity is expressed by the alkyne slip (i.e., unreacted alkyne) rather than conversion. This is the key metric for a purification catalyst, which must operate at conversions approaching 100%; including the slip in the denominator values "complete" alkyne hydrogenation. This value cannot be 0; so, the detection limit of the measurement must be acknowledged and included. Our detection limit is ~0.5 ppm; so, a minimum value of 1 ppm was used when no alkyne was detected. Selectivity is included as the pressure of the undesirable overhydrogenation product in the denominator and as the pressure of alkane, which allows the

https://dx.doi.org/10.1021/acscatal.9b05402
ACS Catal. 2020, 10, 2565−2580

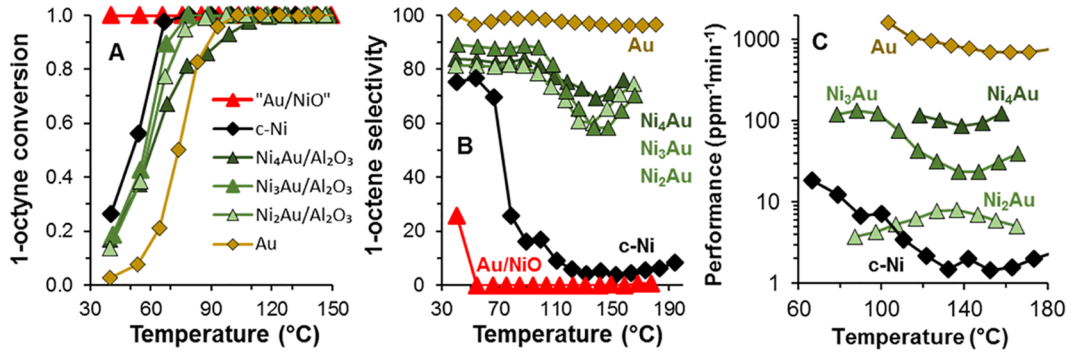

Figure 6. Light-off curves (A), 1-octene selectivity (B), and 1-octene yield (C) for select colloidal catalysts. Conditions: 50 mL/min H_2, 20 Pa 1-octyne, molar space velocities were 10−23 h^{-1}.

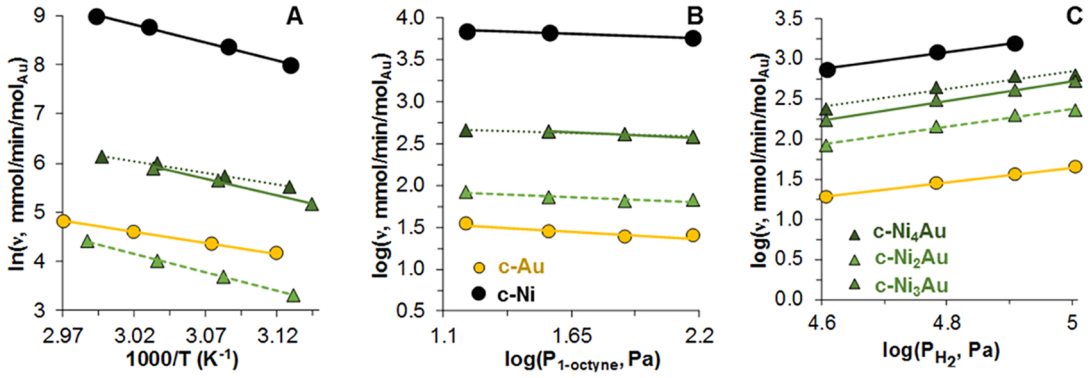

Figure 7. Kinetic plots for Au, Ni, and c-NiAu/Al_2O_3 catalysts. Conditions for Arrhenius plots (A): 50 mL/min H_2, 20 Pa 1-octyne, 40−60 °C. Conditions for 1-octyne order plots (B): 50 mL/min H_2, 20−200 Pa 1-octyne, 60 °C. Conditions for H_2 order plots (C): 20−50 mL/min H_2 (balance to 50 mL/min with N_2), 20 Pa 1-octyne, 60 °C.

expression to be used in cases where alkene is included in the feed.

Figure 5C shows the effects of space velocity on catalyst performance. For clarity, the data included in the plot was limited to points where the 1-octyne slip was less than 5 ppm (>97% conversion); full plots are available in the Supporting Information. At similar space velocities (~20 h^{-1}), Au catalyst performance is 1−2 orders of magnitude better than Ni, due to the high selectivity that is maintained under conditions where alkyne slips are very low. The primary difference is that Au, being less active, requires higher temperatures and lower space velocities to achieve this performance. Figure 5C demonstrates how the performance parameter balances activity and selectivity. At ~150 °C, Ni and Au catalysts have comparable performance; in this case, c-Ni, which is more active, operates at a higher space velocity than Au. The significantly lower selectivity of Ni lowers the overall performance relative to Au, thus indicating that this particular measure of catalyst performance weighs selectivity more heavily than activity.

Low space velocity light-off curve data from the bimetallic c-NiAu catalysts are shown in Figure 6 along with data for a c-Au/NiO control material. The control catalyst was prepared to specifically examine a catalyst where Au interacts with oxidized Ni. In spite of a much lower Au loading (0.2 wt %), c-Au/NiO had a ~100% conversion to the undesired alkane. This is the same result as the commercial NIH Ni catalyst, which was 17 wt % Ni (data in the Supporting Information). The XRD pattern of c-Au/NiO after capping agent removal (see the Supporting Information) showed three sharp peaks at 2θ = 44.5, 51.8, and 76.4° attributable to large Ni(0) particles. This indicates that the H_2/N_2 pretreatment used in removing the oleylamine capping ligands (300 °C, 1 h) resulted in a substantial reduction of the NiO support. We observed similar support reduction with c-Au/Fe_2O_3 catalysts, where the capping ligand removal procedure produced 8−10 nm Fe(0) particles.[48] These results clearly show that Au can serve as a catalyst for NiO or ($Ni_3O_2(OH)_4$) reduction; thus, any oxidized NiO phases in close contact with Au are likely reduced to Ni(0) under catalyst pretreatment conditions. Further, c-Au/NiO catalyst data show the consequence of extended reduced Ni surfaces: high alkyne conversion accompanied by considerable overhydrogenation to the alkane.

The low space velocity c-NiAu light-off curves (Figure 6A) were determined using similar amounts of Ni in the reactor (1−2 μmol Ni) and similar molar space velocities (10−23 h^{-1}). The bimetallic catalysts are slightly less active than Ni, yet more active than Au (measured with 1.6 μmol Au). Alkene selectivity (Figure 6B) was considerably higher than Ni but not as high as Au. Similar to Ni, the bimetallic catalysts showed a propensity for overhydrogenation at higher temperatures, although this deleterious behavior was significantly attenuated relative to the c-Ni catalyst. This resulted in a significantly higher overall performance for the c-NiAu catalysts relative to that for Ni (Figure 6C). The lower selectivity over the bimetallic catalysts resulted in lower overall performance than Au, but the most active sites used only a small fraction of the more expensive metal. Overall, the reactivity data suggest that the catalysis occurs on a Au-modified Ni surface and that Au has a pronounced effect on alkyne partial hydrogenation over Ni.

https://dx.doi.org/10.1021/acscatal.9b05402
ACS Catal. 2020, 10, 2565−2580

Reaction Kinetics. Kinetic parameters were determined under differential reaction conditions to evaluate intrinsic catalyst activity. Although selectivity at high conversion is a more important performance metric for this reaction, the reaction kinetics provide a quantitative comparison of catalyst activity and provide an important check on the consistency of the reaction mechanism across catalysts. Hydrogen and 1-octyne reaction orders, as well as associated observed rate constants (k_{obs}) at 60 °C, and apparent activation barriers (E_{app}) from the Arrhenius studies are compiled in Figure 7 and Table 3. Kinetic data for the commercially available catalysts were similar to the monometallic colloidal catalysts and are included in the Supporting Information.

Reaction orders for all of the catalysts are essentially the same and consistent with the previous studies of monometallic Au catalysts[46,98,99] and with a recent study on a dilute Pd in Au catalyst from Friend and co-workers.[100] The slightly negative alkyne order, coupled with the roughly first-order H_2 dependence, is readily described with a two-site non-competitive reaction mechanism.[48] Alkyne binding is strong and quasi-equilibrated; this results in a reaction limited by hydrogen coverage. The slightly negative alkyne reaction order suggests that the alkyne acts as a weak inhibitor for hydrogen binding. However, this inhibition is sufficiently weak that treating the alkyne dependence as a zero order does not introduce significant error to the extracted kinetic parameters; therefore, the noncompetitive adsorption reaction mechanism remains a reasonable description of the reaction.[48]

The apparent activation energies are relatively similar for all catalysts, ranging from about 40 to 60 kJ/mol. This is similar to the range in E_{app} values (~20 kJ/mol) observed for monometallic Au catalysts on different oxide supports.[48] Given that E_{app} values can vary significantly due to differences in the heat of adsorption values and reactant coverages and that there are no clear trends, it is unlikely that the observed differences are significant. The most important conclusion from the reaction order and Arrhenius studies is the reaction mechanism appears to be consistent over all catalysts. There are no obvious kinetic features enabling distinction between reactions on Ni, Au, or bimetallic NiAu sites. Rather, the kinetic data indicate that the reaction proceeds through similar mechanisms and rate-determining step over all of the catalysts.

Hydrogen Adsorption. The catalysis data indicate that adding a relatively small amount of Au to Ni catalysts has a pronounced effect on alkyne partial hydrogenation, dramatically improving selectivity. Alkene selectivity in this reaction is generally favored by weak alkene and hydrogen binding; both serve to reduce alkene/H coverage and slow undesirable alkene hydrogenation kinetics. We measured H_2 adsorption isotherms as a function of temperature to examine how Au influences hydrogen binding/coverage on Ni.

Figure 8 shows a representative H_2 adsorption experiment for c-Ni, collected at 60 °C. Hydrogen adsorption on c-Ni is dominated by weak adsorption, and relatively little strong chemisorption (difference between the total and reversible isotherms) was measured in the temperature range studied (30−120 °C; see the Supporting Information). There was sufficient H_2 adsorption at all of the temperatures to evaluate the adsorption parameters for strong H_2 chemisorption; linearized Langmuir plots are shown in Figure 8B. This treatment yielded $\Delta H_{ads} = -18 \pm 2$ kJ/mol and $\Delta S_{ads} = -50 \pm 20$ J/(mol K). These values are in excellent agreement with values for H_2 adsorption on a Ni/SiO_2 catalyst prepared via traditional methods ($\Delta H_{ads} = -21 \pm 3$ kJ/mol and $\Delta S_{ads} = -42 \pm 10$ J/(mol K); see the Supporting Information). These values are somewhat lower than what is typically found in the literature,[101−103] suggesting Ni is not fully reduced with this protocol. The conventionally prepared catalyst had higher Ni loading but similar hydrogen uptake per mole of Ni. The Au catalyst showed no strong H_2 adsorption, and the total (weak) adsorption, which was low, increased with temperature (see Figure 9). This is consistent with previous reports and the characterization of H_2 adsorption over Au as "activated adsorption".[104]

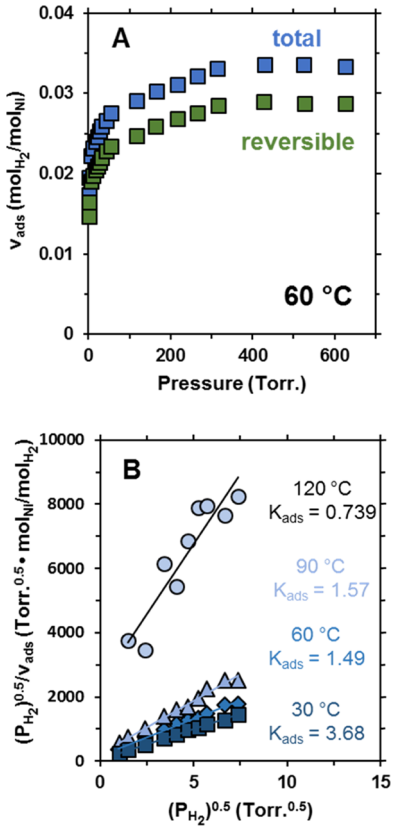

Figure 8. (A) Hydrogen adsorption isotherms on c-Ni collected at 60 °C and (B) linearized strong H_2 adsorption data for c-Ni.

Figure 9 shows the total (i.e., strong + weak/reversible) H_2 adsorption as a function of temperature for all of the catalysts. The total hydrogen adsorption on Ni, after this pretreatment, is not significantly greater than on Au. Taking into account the

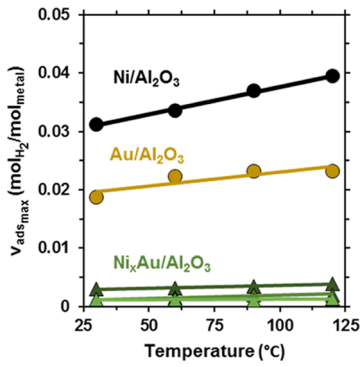

Figure 9. Total hydrogen adsorption as a function of temperature.

https://dx.doi.org/10.1021/acscatal.9b05402
ACS Catal. 2020, 10, 2565−2580

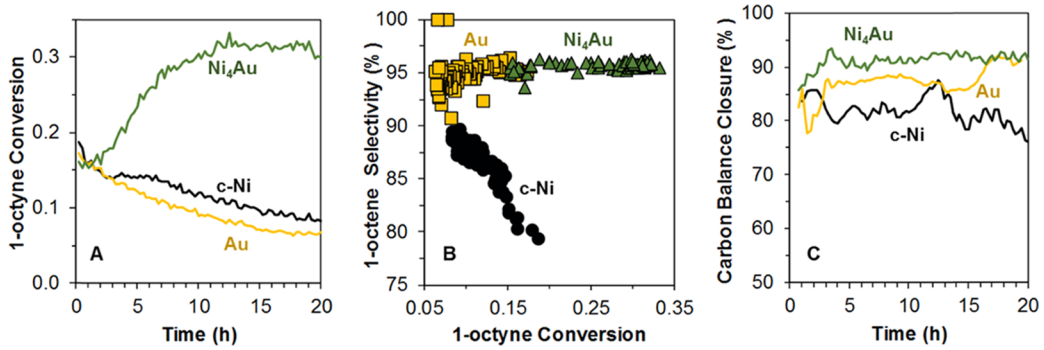

Figure 10. Stability studies for select catalysts: (A) conversion, (B) 1-octene selectivity, and (C) carbon balance. Conditions: 50 mL/min H_2, 90 °C, 20 Pa 1-octyne, ∼0.08 μmol Au for STREM Au and Ni_4Au, ∼0.7 μmol Ni for c-Ni and Ni_4Au; catalyst mass (and hence space velocity) was adjusted so that initial conversions were comparable.

differences in particle size, there are roughly twice as many H_2 adsorption sites on the Ni catalyst. We therefore normalized the kinetic data to the amount of total H_2 adsorption at 60 °C (Table 3). Based on this normalization, the activity of the bimetallic catalysts is roughly in between the monometallic catalysts: approximately 1 order of magnitude faster than Au and little less than an order of magnitude slower than c-Ni.

The bimetallic catalysts have considerably lower H_2 adsorption capacities than the monometallic materials but show the same overall trend of increased H_2 adsorption with temperature. A van't Hoff analysis of the total adsorption (see the Supporting Information) showed no significant trends, with the monometallic and bimetallic catalysts having H_2 adsorption enthalpies ranging from 2 to 7 kJ/mol. Thus, the enthalpy associated with reversible H_2 adsorption is similar for all of the catalysts; the primary difference is in the number of H_2 adsorption sites. It therefore appears that the addition of even small amounts of Au dramatically reduces the number of H_2 adsorption sites on Ni.

Catalyst Stability. Catalyst lifetime and resistance to deactivation are a particularly important property when evaluating the industrial efficacy of lab-generated catalysts. The long-term stability of STREM Au, c-Ni, and c-Ni_3Au was evaluated and is presented in Figure 10A. Catalyst mass/space velocity was adjusted to ensure an initial alkyne conversion of ∼15%. The alkyne conversion of c-Ni and STREM Au behaved similarly: a gradual decline to about 8−10% conversion over 20 h. The alkene selectivity of Au stayed constant at about 95% while the c-Ni started at 80% and slowly rose to 90% as the activity decreased (Figure 10B).

The monometallic catalysts' activity loss is associated with carbon deposition on the catalyst. Figure 10C shows the carbon balance for each catalyst during stability testing. The c-Ni consistently lost ∼20% of the feed alkyne (∼40 ppm) during the 20 h test, presumably due to oligomerization, as Ni catalysts are well known to produce oligomeric side products that deactivate the catalyst.[35] Our choice of a low 1-octyne feed pressure (∼200 ppm) provided greater sensitivity in determining this important catalyst property. The Au catalyst performed slightly better than c-Ni, generally losing 10−15% of the octyne during reaction. Note that for both monometallic catalysts, this corresponded with a 50% reduction in activity.

In contrast, the c-Ni_4Au catalyst maintained relatively stable conversion (∼15%) over the first 2 h. This initial conversion then doubled to 30% over the next 10 h and remained relatively constant for the remainder of the test. This induction period was unique to the bimetallic catalyst. The 1-octene selectivity was both stable and high at ∼95%. The stability of c-Ni_4Au is particularly exciting given the universal problems with catalyst deactivation during selective hydrogenation over both Au and Ni catalysts.

Based on the available literature, Au-containing monometallic and multimetallic hydrogenation catalysts typically lose activity over 12−24 h in bench-scale.[22,42,46,105] We therefore conducted a 7 day stability study using a fresh Ni_4Au sample (Figure 11). As in the previous study, the 1-octyne conversion rose from ∼15 to ∼35% over the first 20 h. Conversion then gradually fell to ∼25% over the next 36 h, and the catalyst remained relatively stable at ∼25% conversion for the duration of the week-long study.

Alkene selectivity for the c-Ni_4Au stability test was between 93 and 97% at all sample points, similar to Figure 10B. In addition, the c-NiAu catalysts' resistance to deactivation corresponded to less carbon loss than observed with the monometallic catalysts. The carbon balance for c-Ni_4Au showed a loss of ∼10−15% (∼20−30 ppm) of the 1-octyne at start-up, presumably due to oligomerization on the catalyst surface. Over the next 24−36 h, the carbon balance closed to within 5%; this corresponded with the ∼2× overall activity increase. The carbon balance continued to close within 5% for the next 6 days, showing a dramatic improvement over either of the two monometallic catalysts.

Correlating the Reactivity and Characterization Data. The reactivity data support a number of conclusions regarding

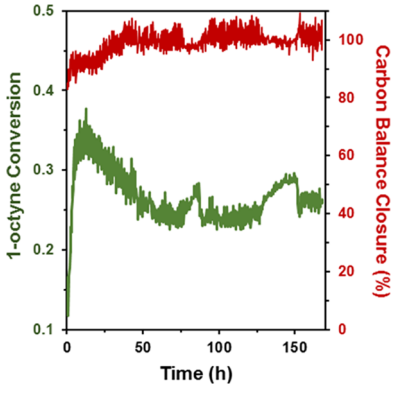

Figure 11. Extended stability study for Ni_4Au/Al_2O_3. The carbon balance is shown in red. Conditions: 50 mL/min H_2, 90 °C, 20 Pa 1-octyne, 2.1 mg catalyst (∼0.08 μmol Au, ∼0.7 μmol Ni), GHSV = 570 000 h^{-1}.

https://dx.doi.org/10.1021/acscatal.9b05402
ACS Catal. 2020, 10, 2565−2580

the reactive surfaces of the bimetallic catalysts under reaction conditions. First, based on the XRD data, after exposure to air, the as-synthesized materials are best described as catalyst precursors in which the synthetic methodology forces a close interaction of Ni and Au. These precursors consist of ~10 nm domains of $(Ni_3O_2(OH)_4)$ dispersed over the alumina support with small Au nanoparticles either embedded in or deposited on the NiO phase. Additional small Au nanoclusters are also dispersed on the alumina. Based on the XRD and reactivity data for the c-Au/NiO catalyst, the Au NPs catalyze the reduction of the $(Ni_3O_2(OH)_4)$ domains during capping agent removal, yielding the active catalyst. Hirata and co-workers similarly observed the Au-catalyzed reduction of NiO,[56−58] and Keane and co-workers used this to dramatically lower the reduction temperatures used in their catalyst preparation.[61,62]

The structural characterization data and the significantly improved alkyne partial hydrogenation performance strongly support the conclusion that the reaction primarily occurs over bimetallic nanoparticles. Based on the lower surface free energy of Au, the bulk immiscibility of Ni and Au, and the higher alkene selectivity, it is likely that Au is located primarily on the nanoparticle surface. However, the EDS data suggests that there is likely a wide range in the relative amounts of surface Au on different particles within the same catalyst, making the consideration of a single active site difficult. We therefore interpret the reactivity data in the context of a simple model of Au adatoms on a reduced Ni surface below, with the understanding that the coverage of Au on Ni likely varies.

We first address the activity of the c-NiAu catalysts. With the exception of the values of the rate constants, the kinetics data are essentially the same on all catalysts. This indicates that the reaction proceeds through similar mechanisms on Au, Ni, and Ni−Au surfaces; however, the number of active sites and the intrinsic activity of those sites differed. Based on the H_2 adsorption data, H coverage on the bimetallic catalysts is significantly lower than on Ni. Since alkyne hydrogenation is rate-limited by hydrogen coverage,[48] the lower rates over the c-NiAu catalysts are consistent with a lower amount of adsorbed H. This could also be considered as Au adatoms poisoning some of the H_2 activation sites on Ni, slowing the catalysis (relative to Ni).

Alkene selectivity is generally associated with two factors: alkene binding energy and hydrogen coverage; in both cases, lower values lead to better alkene selectivity. We consider the intrinsic catalyst selectivity to be the selectivity at about 50% alkyne conversion; this is to distinguish it from the propensity for overhydrogenation, which is associated with selectivity loss at very high conversion. The higher intrinsic selectivity of the c-NiAu catalysts is consistent with lower hydrogen coverage on the bimetallic catalyst surface. This result is also in line with Hardacre and Hu's DFT study, which indicated that decorating a Ni surface with Au decreases alkene binding strength and should increase selectivity.[44] However, the current study does not provide quantitative alkene binding data to test their computational results. At this stage, we simply conclude that the higher intrinsic selectivity is consistent with reactivity on bimetallic surfaces and indicates that most of the Ni surfaces have sufficient Au adatoms to impact both activity and selectivity.

The largest reactivity difference between Ni and Au is in the propensity for overhydrogenation (selectivity loss at high temperatures when conversion is >95%) that occurs with Ni catalysts but is largely absent over Au. The c-NiAu catalysts show a propensity for overhydrogenation, but it is greatly attenuated relative to Ni. This suggests that some of the c-NiAu catalyst surfaces have regions of extended (unmodified) Ni where overhydrogenation can occur. Given the wide range of particle compositions observed in the EDS data, this is consistent with the presence of a small number of monometallic Ni particles with little to no Au coverage.

Finally, stability testing suggests that the bimetallic catalysts undergo some degree of slow morphological change under the reaction environment. The nature of this change is not clear, but we speculate that it is likely associated with the deposition of oligomerization products on the catalyst surface. The mechanistic model that best describes the reaction involves separate sites for alkyne and H_2 binding, with the smaller H_2 molecule being able to access the catalyst surface through "holes" in a porous alkyne overlayer.[48] The deposition of oligomerization products at or near the metal−support interface might block some of the catalyst surface for 1-octyne adsorption, increasing the porosity of the alkyne overlayer. This may, in turn, increase the hydrogen coverage and improve the catalyst activity if the deposits do not block H_2 adsorption to the same degree.

CONCLUSIONS

We developed new synthetic routes to supported Ni and NiAu catalysts using oleylamine and borane *tert*-butylamine. Synthetic conditions were optimized to yield 4.7 ± 0.4 nm particles of oxidized/hydrated Ni. Galvanic displacement of Ni with Au resulted in larger NiO particles that had Au deposited on or embedded in the oxidized Ni. EDS mapping indicated a wide range in the amount of Au associated with the NiO phase, as well as the presence of some small Au particles dispersed throughout the support.

The activity of the NiAu catalysts for the partial hydrogenation of 1-octyne was roughly between the activity of monometallic Ni and Au catalysts. Alkene selectivity was significantly higher than on Ni, although not quite as high as over Au. Notably, the bimetallic catalysts showed a reduced propensity to overhydrogenate the alkene at lower space velocities, resulting in a significantly improved overall catalyst performance. The colloidal preparation method also yielded bimetallic catalysts with dramatically improved resistance to deactivation by oligomerization side products. While Ni and Au monometallic catalysts lost about half of their activity within 20 h, the activity of the bimetallic catalyst improved over this time frame and then remained stable for 1 week.

Based on the activity and selectivity profiles of the c-NiAu catalyst, and comparisons with c-Au/NiO and physical mixture control materials, the active sites are likely composed of bimetallic ensembles, although there may also be some monometallic particles in the c-NiAu catalysts. Hydrogen adsorption data indicate that the catalytically active hydrogen in the system appears to be weakly adsorbed, and the total amount of adsorbed hydrogen increased with temperature. Further, incorporating Au into the bimetallic catalysts dramatically suppresses hydrogen adsorption on Ni. Thus, the improved selectivity of the bimetallic catalysts can be explained, at least, in part, by the lower overall hydrogen coverage, which reduces the rate of alkene hydrogenation.

https://dx.doi.org/10.1021/acscatal.9b05402
ACS Catal. 2020, 10, 2565−2580

■ ASSOCIATED CONTENT

Supporting Information

The Supporting Information is available free of charge at https://pubs.acs.org/doi/10.1021/acscatal.9b05402.

Characterization data (STEM images, particle size distribution histograms, EDS images, IR spectra, and XRD for Au/NiO); catalyst performance and kinetic data for commercial monometallic catalysts; octene yield data for colloidal catalysts on TiO_2, Al_2O_3, and SiO_2; and hydrogen chemisorption data for c-Ni, Ni/Al_2O_3, and Ni/SiO_2 van't Hoff plots (PDF)

■ AUTHOR INFORMATION

Corresponding Author

Bert D. Chandler − *Department of Chemistry, Trinity University, San Antonio, Texas 78240, United States; Laboratorium für Organische Chemie and Laboratorium für Anorganische Chemie, ETH Zürich, CH-8093 Zurich, Switzerland;* orcid.org/0000-0002-8621-0361; Email: bert.chandler@trinity.edu

Authors

James E. Bruno − *Department of Chemistry, Trinity University, San Antonio, Texas 78240, United States*

Nicolas S. Dwarica − *Department of Chemistry, Trinity University, San Antonio, Texas 78240, United States*

Todd N. Whittaker − *Department of Chemistry, Trinity University, San Antonio, Texas 78240, United States*

Emily R. Hand − *Department of Chemistry, Trinity University, San Antonio, Texas 78240, United States*

Clemente S. Guzman, IV − *Department of Chemistry, Trinity University, San Antonio, Texas 78240, United States*

Anish Dasgupta − *Department of Chemical Engineering, The Pennsylvania State University, University Park, Pennsylvania 16802, United States*

Zhifeng Chen − *Department of Chemical Engineering, The Pennsylvania State University, University Park, Pennsylvania 16802, United States*

Robert M. Rioux − *Department of Chemical Engineering and Department of Chemistry, The Pennsylvania State University, University Park, Pennsylvania 16802, United States;* orcid.org/0000-0002-6019-0032

Complete contact information is available at: https://pubs.acs.org/10.1021/acscatal.9b05402

Notes

The authors declare no competing financial interest.

■ ACKNOWLEDGMENTS

The authors gratefully acknowledge the National Science Foundation (Grants CHE-1566301 and CBET-1803769) and the Research Corporation for Science Advancement for support of this work. The alumina support was generously provided by Sasol. The authors specially thank Gary Gildert (Vanguard Catalyst) for donating the commercial NIH Ni/Al_2O_3 catalyst and providing technical expertise. B.D.C. thanks Profs. Jeff Bode and Christophe Copéret as well as the Laboratorium für Organische Chemie and the Laboratorium für Anorganische Chemie at ETH Zürich for support during his academic leave. C.S.G. also thanks the Trinity University McNair Scholar program for additional support.

■ REFERENCES

(1) Lopez-Sanchez, J. A.; Lennon, D. The use of titania- and iron oxide-supported gold catalysts for the hydrogenation of propyne. *Appl. Catal., A* **2005**, *291*, 230−237.

(2) Hugon, A.; Delannoy, L.; Louis, C. Supported gold catalysts for selective hydrogenation of 1,3-butadiene in the presence of an excess of alkenes. *Gold Bull.* **2008**, *41*, 127−138.

(3) Vilé, G.; Pérez-Ramírez, J. Beyond the use of modifiers in selective alkyne hydrogenation: silver and gold nanocatalysts in flow mode for sustainable alkene production. *Nanoscale* **2014**, *6*, 13476−13482.

(4) Nikolaev, S. A.; Permyakov, N. A.; Smirnov, V. V.; Vasil'kov, A. Y.; Lanin, S. N. Selective hydrogenation of phenylacetylene into styrene on gold nanoparticles. *Kinet. Catal.* **2010**, *51*, 288−292.

(5) Borodziński, A.; Bond, G. C. Selective Hydrogenation of Ethyne in Ethene-Rich Streams on Palladium Catalysts. Part 1. Effect of Changes to the Catalyst During Reaction. *Catal. Rev.* **2006**, *48*, 91−144.

(6) Borodziński, A.; Bond, G. C. Selective Hydrogenation of Ethyne in Ethene-Rich Streams on Palladium Catalysts, Part 2: Steady-State Kinetics and Effects of Palladium Particle Size, Carbon Monoxide, and Promoters. *Catal. Rev.* **2008**, *50*, 379−469.

(7) Yardimci, D.; Serna, P.; Gates, B. C. Tuning Catalytic Selectivity: Zeolite- and Magnesium Oxide-Supported Molecular Rhodium Catalysts for Hydrogenation of 1,3-Butadiene. *ACS Catal.* **2012**, *2*, 2100−2113.

(8) Schbib, N. S.; García, M. A.; Gígola, C. E.; Errazu, A. F. Kinetics of Front-End Acetylene Hydrogenation in Ethylene Production. *Ind. Eng. Chem. Res.* **1996**, *35*, 1496−1505.

(9) Studt, F.; Abild-Pedersen, F.; Bligaard, T.; Sørensen, R. Z.; Christensen, C. H.; Nørskov, J. K. Identification of Non-Precious Metal Alloy Catalysts for Selective Hydrogenation of Acetylene. *Science* **2008**, *320*, 1320.

(10) McCue, A. J.; Anderson, J. A. Recent advances in selective acetylene hydrogenation using palladium containing catalysts. *Front. Chem. Sci. Eng.* **2015**, *9*, 142−153.

(11) Asplund, S. Coke Formation and Its Effect on Internal Mass Transfer and Selectivity in Pd-Catalysed Acetylene Hydrogenation. *J. Catal.* **1996**, *158*, 267−278.

(12) Sárkány, A.; Guczi, L.; Weiss, A. H. On the aging phenomenon in palladium catalysed acetylene hydrogenation. *Appl. Catal.* **1984**, *10*, 369−388.

(13) Ravanchi, M. T.; Sahebdelfar, S.; Fard, M. R.; Fadaeerayeni, S.; Bigdeli, P. Pd-Ag/α-Al2O3 Catalyst Deactivation in Acetylene Selective Hydrogenation Process. *Chem. Eng. Technol.* **2016**, *39*, 301−310.

(14) Li, Y.; Jang, B. W. L. Selective Hydrogenation of Acetylene Over Pd/Al2O3 Catalysts: Effect of Non-thermal RF Plasma Preparation Methodologies. *Top. Catal.* **2017**, *60*, 997−1008.

(15) Yan, H.; Cheng, H.; Yi, H.; Lin, Y.; Yao, T.; Wang, C.; Li, J.; Wei, S.; Lu, J. Single-Atom Pd1/Graphene Catalyst Achieved by Atomic Layer Deposition: Remarkable Performance in Selective Hydrogenation of 1,3-Butadiene. *J. Am. Chem. Soc.* **2015**, *137*, 10484−10487.

(16) Castillejos-López, E.; Agostini, G.; Di Michel, M.; Iglesias-Juez, A.; Bachiller-Baeza, B. Synergy of Contact between ZnO Surface Planes and PdZn Nanostructures: Morphology and Chemical Property Effects in the Intermetallic Sites for Selective 1,3-Butadiene Hydrogenation. *ACS Catal.* **2017**, *7*, 796−811.

(17) Tew, M. W.; Emerich, H.; van Bokhoven, J. A. Formation and Characterization of PdZn Alloy: A Very Selective Catalyst for Alkyne Semihydrogenation. *J. Phys. Chem. C* **2011**, *115*, 8457−8465.

(18) Giedigkeit, R.; Armbruester, M.; Kovnir, K.; Grin, J.; Schloegl, R.; Osswald, J.; Ressler, T.; Jentoft, R. E. Hydrogenation Process Using Catalyst Comprising Ordered Intermetallic Compound. European PatentEP18349392007.

(19) Kyriakou, G.; Boucher, M. B.; Jewell, A. D.; Lewis, E. A.; Lawton, T. J.; Baber, A. E.; Tierney, H. L.; Flytzani-Stephanopoulos,

M.; Sykes, E. C. H. Isolated Metal Atom Geometries as a Strategy for Selective Heterogeneous Hydrogenations. *Science* **2012**, *335*, 1209.
(20) Pei, G.; Liu, X.; Chai, M.; Wang, A.; Zhang, T. Isolation of Pd atoms by Cu for semi-hydrogenation of acetylene: Effects of Cu loading. *Chin. J. Catal.* **2017**, *38*, 1540−1548.
(21) Boucher, M. B.; Zugic, B.; Cladaras, G.; Kammert, J.; Marcinkowski, M. D.; Lawton, T. J.; Sykes, E. C. H.; Flytzani-Stephanopoulos, M. Single atom alloy surface analogs in Pd0.18Cu15 nanoparticles for selective hydrogenation reactions. *Phys. Chem. Chem. Phys.* **2013**, *15*, 12187−12196.
(22) Ma, C.; Du, Y.; Feng, J.; Cao, X.; Yang, J.; Li, D. Fabrication of supported PdAu nanoflower catalyst for partial hydrogenation of acetylene. *J. Catal.* **2014**, *317*, 263−271.
(23) Kruppe, C. M.; Krooswyk, J. D.; Trenary, M. Selective Hydrogenation of Acetylene to Ethylene in the Presence of a Carbonaceous Surface Layer on a Pd/Cu(111) Single-Atom Alloy. *ACS Catal.* **2017**, *7*, 8042−8049.
(24) Pei, G. X.; Liu, X. Y.; Yang, X.; Zhang, L.; Wang, A.; Li, L.; Wang, H.; Wang, X.; Zhang, T. Performance of Cu-Alloyed Pd Single-Atom Catalyst for Semihydrogenation of Acetylene under Simulated Front-End Conditions. *ACS Catal.* **2017**, *7*, 1491−1500.
(25) Pei, G. X.; Liu, X. Y.; Wang, A.; Li, L.; Huang, Y.; Zhang, T.; Lee, J. W.; Jang, B. W. L.; Mou, C.-Y. Promotional effect of Pd single atoms on Au nanoparticles supported on silica for the selective hydrogenation of acetylene in excess ethylene. *New J. Chem.* **2014**, *38*, 2043−2051.
(26) Yang, B.; Burch, R.; Hardacre, C.; Headdock, G.; Hu, P. Influence of surface structures, subsurface carbon and hydrogen, and surface alloying on the activity and selectivity of acetylene hydrogenation on Pd surfaces: A density functional theory study. *J. Catal.* **2013**, *305*, 264−276.
(27) Feng, J.; Liu, Y.; Yin, M.; He, Y.; Zhao, J.; Sun, J.; Li, D. Preparation and structure-property relationships of supported trimetallic PdAuAg catalysts for the selective hydrogenation of acetylene. *J. Catal.* **2016**, *344*, 854−864.
(28) Yan, X.; Bao, J.; Yuan, C.; Wheeler, J.; Lin, W.-Y.; Li, R.; Jang, B. W. L. Gold on carbon and titanium oxides composites: Highly efficient and stable acetylene hydrogenation in large excess of ethylene. *J. Catal.* **2016**, *344*, 194−201.
(29) Concepción, P.; García, S.; Hernández-Garrido, J. C.; Calvino, J. J.; Corma, A. A promoting effect of dilution of Pd sites due to gold surface segregation under reaction conditions on supported Pd−Au catalysts for the selective hydrogenation of 1,5-cyclooctadiene. *Catal. Today* **2016**, *259*, 213−221.
(30) Hugon, A.; Delannoy, L.; Krafft, J.-M.; Louis, C. Selective Hydrogenation of 1,3-Butadiene in the Presence of an Excess of Alkenes over Supported Bimetallic Gold−Palladium Catalysts. *J. Phys. Chem. C* **2010**, *114*, 10823−10835.
(31) Liu, J.; Shan, J.; Lucci, F. R.; Cao, S.; Sykes, E. C. H.; Flytzani-Stephanopoulos, M. Palladium−gold single atom alloy catalysts for liquid phase selective hydrogenation of 1-hexyne. *Catal. Sci. Technol.* **2017**, *7*, 4276−4284.
(32) Blankenship, S. A.; Vioight, R. W.; Perkins, J. A.; Fried, J.; James, E. Process for the Selective Hydrogenation of Acetylene in an Ethylene Purification Stream. U.S. PatentUS65092922003.
(33) Zimmermann, R. R.; Hahn, T.; Reschetilowski, W.; Armbrüster, M. Kinetic Parameters for the Selective Hydrogenation of Acetylene on GaPd2 and GaPd. *ChemPhysChem* **2017**, *18*, 2517−2525.
(34) Johnson, M. M.; Walker, D. W.; Nowack, G. P. Selective Hydrogenation Catalyst. U.S. Patent US4404124A1983.
(35) Spanjers, C. S.; Held, J. T.; Jones, M. J.; Stanley, D. D.; Sim, R. S.; Janik, M. J.; Rioux, R. M. Zinc inclusion to heterogeneous nickel catalysts reduces oligomerization during the semi-hydrogenation of acetylene. *J. Catal.* **2014**, *316*, 164−173.
(36) Dai, X.; Chen, Z.; Yao, T.; Zheng, L.; Lin, Y.; Liu, W.; Ju, H.; Zhu, J.; Hong, X.; Wei, S.; Wu, Y.; Li, Y. Single Ni sites distributed on N-doped carbon for selective hydrogenation of acetylene. *Chem. Commun.* **2017**, *53*, 11568−11571.
(37) Riley, C.; Riva, A. D. L.; Zhou, A.; Wan, S.; Peterson, Q.; Artyushkova, E.; Farahani, K.; Friedrich, M. D.; Burkemper, H. B.; Atudorei, L.; Lin, N.-V.; Guo, S.; Datye, H. Synthesis of Nickel-Doped Ceria Catalysts for Selective Acetylene Hydrogenation. *ChemCatChem* **2019**, *11*, 1526−1533.
(38) Riley, C.; Zhou, S.; Kunwar, D.; De La Riva, A.; Peterson, E.; Payne, R.; Gao, L.; Lin, S.; Guo, H.; Datye, A. Design of Effective Catalysts for Selective Alkyne Hydrogenation by Doping of Ceria with a Single-Atom Promotor. *J. Am. Chem. Soc.* **2018**, *140*, 12964−12973.
(39) Azizi, Y.; Petit, C.; Pitchon, V. Formation of polymer-grade ethylene by selective hydrogenation of acetylene over Au/CeO2 catalyst. *J. Catal.* **2008**, *256*, 338−344.
(40) Gluhoi, A. C.; Bakker, J. W.; Nieuwenhuys, B. E. Gold, still a surprising catalyst: Selective hydrogenation of acetylene to ethylene over Au nanoparticles. *Catal. Today* **2010**, *154*, 13−20.
(41) Jia, J.; Haraki, K.; Kondo, J. N.; Domen, K.; Tamaru, K. Selective Hydrogenation of Acetylene over Au/Al2O3 Catalyst. *J. Phys. Chem. B* **2000**, *104*, 11153−11156.
(42) Yan, X.; Wheeler, J.; Jang, B.; Lin, W.-Y.; Zhao, B. Stable Au catalysts for selective hydrogenation of acetylene in ethylene. *Appl. Catal., A* **2014**, *487*, 36−44.
(43) Segura, Y.; López, N.; Pérez-Ramírez, J. Origin of the superior hydrogenation selectivity of gold nanoparticles in alkyne + alkene mixtures: Triple- versus double-bond activation. *J. Catal.* **2007**, *247*, 383−386.
(44) Yang, B.; Burch, R.; Hardacre, C.; Headdock, G.; Hu, P. Origin of the Increase of Activity and Selectivity of Nickel Doped by Au, Ag, and Cu for Acetylene Hydrogenation. *ACS Catal.* **2012**, *2*, 1027−1032.
(45) Hugon, A.; Delannoy, L.; Louis, C. Influence of the reactant concentration in selective hydrogenation of 1,3-butadiene over supported gold catalysts under alkene rich conditions: A consideration of reaction mechanism. *Gold Bull.* **2009**, *42*, 310−320.
(46) Masoud, N.; Delannoy, L.; Schaink, H. L.; Van der Eerden, A. M. J.; de Rijk, J.-W.; Silva, T. A. G.; Banerjee, D.; Meeldijk, J. D.; de Jong, K. P.; Louis, C.; de Jongh, P. E. On the Superior Stability of Au/SiO2 Compared to Au/TiO2 Catalysts for the Selective Hydrogenation of Butadiene. *ACS Catal.* **2017**, *7*, 5594−5603.
(47) Shao, L.; Huang, X.; Teschner, D.; Zhang, W. Gold Supported on Graphene Oxide: An Active and Selective Catalyst for Phenylacetylene Hydrogenations at Low Temperatures. *ACS Catal.* **2014**, *4*, 2369−2373.
(48) Bruno, J. E.; Sravan Kumar, K. B.; Dwarica, N. S.; Hüther, A.; Chen, Z.; Guzman, C. S., IV; Hand, E. R.; Moore, W. C.; Rioux, R. M.; Grabow, L. C.; Chandler, B. D. On the Limited Role of Electronic Support Effects in Selective Alkyne Hydrogenation: A Kinetic Study of Au/MOx Catalysts Prepared from Oleylamine-Capped Colloidal Nanoparticles. *ChemCatChem* **2019**, *11*, 1650−1664.
(49) Sárkány, A. Acetylene hydrogenation on SiO2 supported gold nanoparticles. *React. Kinet. Catal. Lett.* **2009**, *96*, 43−54.
(50) Boronat, M.; Concepción, P.; Corma, A. Unravelling the Nature of Gold Surface Sites by Combining IR Spectroscopy and DFT Calculations. Implications in Catalysis. *J. Phys. Chem. C* **2009**, *113*, 16772−16784.
(51) Bus, E.; Miller, J. T.; van Bokhoven, J. A. Hydrogen Chemisorption on Al2O3-Supported Gold Catalysts. *J. Phys. Chem. B* **2005**, *109*, 14581−14587.
(52) Fujitani, T.; Nakamura, I.; Akita, T.; Okumura, M.; Haruta, M. Hydrogen Dissociation by Gold Clusters. *Angew. Chem.* **2009**, *121*, 9679−9682.
(53) Ward, T.; Delannoy, L.; Hahn, R.; Kendell, S.; Pursell, C. J.; Louis, C.; Chandler, B. D. Effects of Pd on Catalysis by Au: CO Adsorption, CO Oxidation, and Cyclohexene Hydrogenation by Supported Au and Pd-Au Catalysts. *ACS Catal.* **2013**, *3*, 2644−2653.
(54) Hugon, A.; Delannoy, L.; Krafft, J.-M.; Louis, C. Selective Hydrogenation of 1,3-Butadiene in the Presence of an Excess of Alkenes over Supported Bimetallic Gold-Palladium Catalysts. *J. Phys. Chem. C* **2010**, *114*, 10823−10835.

https://dx.doi.org/10.1021/acscatal.9b05402
ACS Catal. 2020, 10, 2565−2580

(55) Herz, A.; Wang, D.; Kups, T.; Schaaf, P. Solid-state dewetting of Au/Ni bilayers: The effect of alloying on morphology evolution. *J. Appl. Phys.* **2014**, *116*, No. 044307.
(56) Hirata, H. Recent Research Progress in Automotive Exhaust Gas Purification Catalyst. *Catal. Surv. Asia* **2014**, *18*, 128−133.
(57) Shirakawa, S.; Osaki, M.; Nagai, Y.; Nishimura, Y. F.; Dohmae, K.; Matsumoto, Si.; Hirata, H. XAFS study on promoting effect of Au via NiO reduction in Au-Ni bimetallic clusters. *Catal. Today* **2017**, *281*, 429−436.
(58) Beniya, A.; Ikuta, Y.; Isomura, N.; Hirata, H.; Watanabe, Y. Synergistic Promotion of NO-CO Reaction Cycle by Gold and Nickel Elucidated using a Well-Defined Model Bimetallic Catalyst Surface. *ACS Catal.* **2017**, *7*, 1369−1377.
(59) Kyriakou, G.; Márquez, A. M.; Holgado, J. P.; Taylor, M. J.; Wheatley, A. E. H.; Mehta, J. P.; Fernández Sanz, J.; Beaumont, S. K.; Lambert, R. M. Comprehensive Experimental and Theoretical Study of the CO + NO Reaction Catalyzed by Au/Ni Nanoparticles. *ACS Catal.* **2019**, *9*, 4919−4929.
(60) Cárdenas-Lizana, F.; Gómez-Quero, S.; Keane, M. A. Gas Phase Hydrogenation of m-Dinitrobenzene over Alumina Supported Au and Au−Ni Alloy. *Catal. Lett.* **2009**, *127*, 25−32.
(61) Cárdenas-Lizana, F.; Gómez-Quero, S.; Baddeley, C. J.; Keane, M. A. Tunable gas phase hydrogenation of m-dinitrobenzene over alumina supported Au and Au−Ni. *Appl. Catal., A* **2010**, *387*, 155−165.
(62) Cárdenas-Lizana, F.; Keane, M. A. Gas phase selective hydrogenation over oxide supported Ni−Au. *Phys. Chem. Chem. Phys.* **2015**, *17*, 28088−28095.
(63) Qin, L.; Zeng, Z.; Zeng, G.; Lai, C.; Duan, A.; Xiao, R.; Huang, D.; Fu, Y.; Yi, H.; Li, B.; Liu, X.; Liu, S.; Zhang, M.; Jiang, D. Cooperative catalytic performance of bimetallic Ni−Au nanocatalyst for highly efficient hydrogenation of nitroaromatics and corresponding mechanism insight. *Appl. Catal., B* **2019**, *259*, No. 118035.
(64) Lamey, D.; Beswick, O.; Cárdenas-Lizana, F.; Dyson, P. J.; Sulman, E.; Kiwi-Minsker, L. Highly selective immobilized bimetallic Ni-Au nanoparticle catalyst for the partial hydrogenation of m-dinitrobenzene. *Appl. Catal., A* **2017**, *542*, 182−190.
(65) Chai, M.; Liu, X.; Li, L.; Pei, G.; Ren, Y.; Su, Y.; Cheng, H.; Wang, A.; Zhang, T. SiO2-supported Au-Ni bimetallic catalyst for the selective hydrogenation of acetylene. *Chin. J. Catal.* **2017**, *38*, 1338−1346.
(66) Nikolaev, S. A.; Smirnov, V. V.; Vasil'kov, A. Y.; Podshibikhin, V. L. Synergism of the catalytic effect of nanosized gold-nickel catalysts in the reaction of selective acetylene hydrogenation to ethylene. *Kinet. Catal.* **2010**, *51*, 375−379.
(67) Nikolaev, S. A.; Smirnov, V. V. Synergistic and size effects in selective hydrogenation of alkynes on gold nanocomposites. *Catal. Today* **2009**, *147*, S336−S341.
(68) Aguilar-Tapia, A.; Delannoy, L.; Louis, C.; Han, C. W.; Ortalan, V.; Zanella, R. Selective hydrogenation of 1,3-butadiene over bimetallic Au-Ni/TiO2 catalysts prepared by deposition-precipitation with urea. *J. Catal.* **2016**, *344*, 515−523.
(69) Keane, M. A.; Gomez-Quero, S.; Cardenas-Lizana, F.; Shen, W. Alumina-Supported Ni-Au: Surface Synergistic Effects in Catalytic Hydrodechlorination. *ChemCatChem* **2009**, *1*, 270−278.
(70) Tkachenko, O. P.; Kustov, L. M.; Nikolaev, S. A.; Smirnov, V. V.; Klementiev, K. V.; Naumkin, A. V.; Volkov, I. O.; Vasil'kov, A. Y.; Murzin, D. Y. DRIFT, XPS and XAS Investigation of Au−Ni/Al2O3 Synergetic Catalyst for Allylbenzene Isomerization. *Top. Catal.* **2009**, *52*, 344−350.
(71) Chandler, B. D.; Long, C. G.; Gilbertson, J. D.; Vijayaraghavan, G.; Stevenson, K. J.; Pursell, C. J. Improving Oxygen Activation Over Supported Au Catalysts Through the Controlled Preparation of Bimetallic Ni-Au Nanoparticles. *J. Phys. Chem. C* **2010**, *114*, 11498−11508.
(72) Lahr, D. L.; Ceyer, S. T. Catalyzed CO Oxidation at 70 K on an Extended Au/Ni Surface Alloy. *J. Am. Chem. Soc.* **2006**, *128*, 1800−1801.
(73) Leon, C. C.; Lee, J.-G.; Ceyer, S. T. Oxygen Adsorption on Au−Ni(111) Surface Alloys. *J. Phys. Chem. C* **2014**, *118*, 29043−29057.
(74) Leon, C. C.; Liu, Q.; Ceyer, S. T. CO Adsorption on Gold Nickel Au−Ni(111) Surface Alloys. *J. Phys. Chem. C* **2019**, *123*, 9041−9058.
(75) Guo, J.; Dong, F.; Zhong, S.; Zhu, B.; Huang, W.; Zhang, S. Effect of Ni Addition on the Low Temperature Carbon Monoxide Oxidation over Au/HAP Nanocatalyst. *Catal. Surv. Asia* **2018**, *22*, 208−221.
(76) Yi, W.; Yuan, W.; Meng, Y.; Zou, S.; Zhou, Y.; Hong, W.; Che, J.; Hao, M.; Ye, B.; Xiao, L.; Wang, Y.; Kobayashi, H.; Fan, J. A Rational Solid-State Synthesis of Supported Au−Ni Bimetallic Nanoparticles with Enhanced Activity for Gas-Phase Selective Oxidation of Alcohols. *ACS Appl. Mater. Interfaces* **2017**, *9*, 31853−31860.
(77) Ruppert, A. M.; Jędrzejczyk, M.; Potrzebowska, N.; Kaźmierczak, K.; Brzezińska, M.; Sneka-Płatek, O.; Sautet, P.; Keller, N.; Michel, C.; Grams, J. Supported gold−nickel nano-alloy as a highly efficient catalyst in levulinic acid hydrogenation with formic acid as an internal hydrogen source. *Catal. Sci. Technol.* **2018**, *8*, 4318−4331.
(78) Giannakakis, G.; Trimpalis, A.; Shan, J.; Qi, Z.; Cao, S.; Liu, J.; Ye, J.; Biener, J.; Flytzani-Stephanopoulos, M. NiAu Single Atom Alloys for the Non-oxidative Dehydrogenation of Ethanol to Acetaldehyde and Hydrogen. *Top. Catal.* **2018**, *61*, 475−486.
(79) Xu, X.; Fu, Q.; Guo, X.; Bao, X. A Highly Active "NiO-on-Au" Surface Architecture for CO Oxidation. *ACS Catal.* **2013**, *3*, 1810−1818.
(80) Auten, B. J.; Hahn, B. P.; Vijayaraghavan, G.; Stevenson, K. J.; Chandler, B. D. Preparation and Characterization of 3 nm Magnetic NiAu Nanoparticles. *J. Phys. Chem. C* **2008**, *112*, 5365−5372.
(81) Zhou, S.; Ma, Z.; Yin, H.; Wu, Z.; Eichhorn, B.; Overbury, S. H.; Dai, S. Low-Temperature Solution-Phase Synthesis of NiAu Alloy Nanoparticles via Butyllithium Reduction: Influences of Synthesis Details and Application As the Precursor to Active Au-NiO/SiO2 Catalysts through Proper Pretreatment. *J. Phys. Chem. C* **2009**, *113*, 5758−5765.
(82) Korkosz, R. J.; Gilbertson, J. D.; Prasifka, K. S.; Chandler, B. D. Dendrimer Templates for Supported Au Catalysts. *Catal. Today* **2007**, *122*, 370−377.
(83) Gilbertson, J. D.; Vijayaraghavan, G.; Stevenson, K. J.; Chandler, B. D. Air and Water Free Solid Phase Synthesis of Thiol Stabilized Au Nanoparticles with Anchored, Recyclable Dendrimer Templates. *Langmuir* **2007**, *23*, 11239−11245.
(84) Nishikawa, H.; Kawamoto, D.; Yamamoto, Y.; Ishida, T.; Ohashi, H.; Akita, T.; Honma, T.; Oji, H.; Kobayashi, Y.; Hamasaki, A.; Yokoyama, T.; Tokunaga, M. Promotional effect of Au on reduction of Ni(II) to form Au−Ni alloy catalysts for hydrogenolysis of benzylic alcohols. *J. Catal.* **2013**, *307*, 254−264.
(85) Charles, R. G.; Pawlikowski, M. A. Comparative Heat Stabilities of Some Metal Acetylacetonate Chelates. *J. Phys. Chem. A.* **1958**, *62*, 440−444.
(86) Glemster, O.; Sauer, H. Section 19: Copper, Silver, Gold. In *Handbook of Preparative Inorganic Chemistry*; BRAUER, G., Ed.; Academic press: New York, 1965; Vol. 2, pp 1003−1065.
(87) Peng, S.; Lee, Y.; Wang, C.; Yin, H.; Dai, S.; Sun, S. A facile synthesis of monodisperse Au nanoparticles and their catalysis of CO oxidation. *Nano Res.* **2008**, *1*, 229−234.
(88) Chandler, B. D.; Gilbertson, J. D. Dendrimer-Encapsulated Bimetallic Nanoparticles: Synthesis, Characterization, and Applications to Homogeneous and Heterogeneous Catalysis. In *Topics in Organometallic Chem.: Dendrimer Catalysis*; Gade, L., Ed.; Springer, 2006; Vol. *21*, pp 97−120.
(89) Singh, A.; Chandler, B. D. Mild Thermolysis Conditions for the Activation of Dendrimer Encapsulated Pt Nanoparticles. *Langmuir* **2005**, *21*, 10776−10782.

https://dx.doi.org/10.1021/acscatal.9b05402
ACS Catal. 2020, 10, 2565−2580

(90) Landry, A. M.; Iglesia, E. Displacement-reduction routes to PtPd clusters and mechanistic inferences for the synthesis of other bimetallic compositions. *J. Catal.* **2016**, *344*, 389−400.
(91) Whittaker, T.; Kanchari Bavajigari, S. K.; Peterson, C.; Pollock, M. N.; Grabow, L. C.; Chandler, B. D. H2 Oxidation over Supported Au Nanoparticle Catalysts: Evidence for Heterolytic H2 Activation at the Metal-Support Interface. *J. Am. Chem. Soc.* **2018**, *140*, 16469−16487.
(92) Cargnello, M.; Doan-Nguyen, V. V. T.; Gordon, T. R.; Diaz, R. E.; Stach, E. A.; Gorte, R. J.; Fornasiero, P.; Murray, C. B. Control of Metal Nanocrystal Size Reveals Metal-Support Interface Role for Ceria Catalysts. *Science* **2013**, *341*, 771−773.
(93) Metin, Ö.; Mazumder, V.; Özkar, S.; Sun, S. Monodisperse Nickel Nanoparticles and Their Catalysis in Hydrolytic Dehydrogenation of Ammonia Borane. *J. Am. Chem. Soc.* **2010**, *132*, 1468−1469.
(94) Knecht, M. R.; Garcia-Martinez, J. C.; Crooks, R. M. Synthesis, Characterization, and Magnetic Properties of Denrimer-Encapsulated Nickel Nanoparticles Containing <150 Atoms. *Chem. Mater.* **2006**, *18*, 5039−5044.
(95) Cardenas-Lizana, F.; Gomez-Quero, S.; Jacobs, G.; Ji, Y.; Davis, B. H.; Kiwi-Minsker, L.; Keane, M. A. Alumina Supported Au-Ni: Surface Synergism in the Gas Phase Hydrogenation of Nitro-Compounds. *J. Phys. Chem. C* **2012**, *116*, 11166−11180.
(96) Spanjers, C. S.; Held, J. T.; Jones, M. J.; Stanley, D. D.; Sim, R. S.; Janik, M. J.; Rioux, R. M. Zinc inclusion to heterogeneous nickel catalysts reduces oligomerization during the semi-hydrogenation of acetylene. *J. Catal.* **2014**, *316*, 164−173.
(97) Saavedra, J.; Whittaker, T.; Chen, Z.; Pursell, C. J.; Rioux, R. M.; Chandler, B. D. Controlling activity and selectivity using water in the Au-catalysed preferential oxidation of CO in H2. *Nat. Chem.* **2016**, *8*, 584−589.
(98) Bruno, J. E.; Kumar, K. B. S.; Dwarica, N. S.; Hüther, A.; Chen, Z.; Guzman, C. S.; Hand, E. R.; Moore, W. C.; Rioux, R. M.; Grabow, L. C.; Chandler, B. D. On the Limited Role of Electronic Support Effects in Selective Alkyne Hydrogenation: A Kinetic Study of Au/MOx Catalysts Prepared from Oleylamine-Capped Colloidal Nanoparticles. *ChemCatChem* 1650 1664. DOI: 10.1002/cctc.201801882.
(99) Neurock, M.; van Santen, R. A. A First Principles Analysis of C−H Bond Formation in Ethylene Hydrogenation. *J. Phys. Chem. B* **2000**, *104*, 11127−11145.
(100) Luneau, M.; Shirman, T.; Foucher, A. C.; Duanmu, K.; Verbart, D. M. A.; Sautet, P.; Stach, E. A.; Aizenberg, J.; Madix, R. J.; Friend, C. M. Achieving High Selectivity for Alkyne Hydrogenation at High Conversions with Compositionally Optimized PdAu Nanoparticle Catalysts in Raspberry Colloid-Templated SiO2. *ACS Catal.* **2020**, *10*, 441−450.
(101) Weatherbee, G. D.; Bartholomew, C. H. Effects of support on hydrogen adsorption/desorption kinetics of nickel. *J. Catal.* **1984**, *87*, 55−65.
(102) Smeds, S.; Salmi, T.; Lindfors, L. P.; Krause, O. Chemisorption and TPD studies of hydrogen on Ni/Al2O3. *Appl. Catal., A* **1996**, *144*, 177−194.
(103) Bradford, M. C. J.; Vannice, M. A. Catalytic reforming of methane with carbon dioxide over nickel catalysts I. Catalyst characterization and activity. *Appl. Catal., A* **1996**, *142*, 73−96.
(104) Bus, E.; Miller, J. T.; van Bokhoven, J. A. Hydrogen Chemisorption on Al2O3-Supported Gold Catalysts. *J. Phys. Chem. B* **2005**, *109*, 14581−14587.
(105) Zhang, S.; Chen, C.-Y.; Jang, B. W. L.; Zhu, A.-M. Radio-frequency H2 plasma treatment of AuPd/TiO2 catalyst for selective hydrogenation of acetylene in excess ethylene. *Catal. Today* **2015**, *256*, 161−169.

https://dx.doi.org/10.1021/acscatal.9b05402
ACS Catal. 2020, 10, 2565−2580